CERN-ACC-NOTE-2018-0006

15 February 2018
mfittere@fnal.gov

MD1271: Effect of low frequency noise on the evolution of the emittance and halo population

M. Fitterer, G. Stancari, A. Valishev (Fermilab), R. Bruce, W. Höfle, M. Hostettler, S. P. Papadopoulou, G. Papotti, Y. Papaphilippou, D. Pellegrini, G. Trad, D. Valuch, G. Valentino, J. Wagner, C. Xu, CERN, Geneva Switzerland

Keywords: ground motion, noise, emittance, halo population

Summary

For the High Luminosity upgrade the β^* in IR1 and IR5 will be further reduced compared to the current LHC. As the β^* decreases the β-functions in the inner triplet (IT) increase resulting in a higher sensitivity of the HL-LHC to ground motion in the IT region or to increases of the low frequency noise. Noise can in general lead to emittance growth and higher halo population and diffusion rate. However, it is usually assumed in the literature that only frequencies close to the betatron frequencies and sidebands have an effect on the emittance and tail population. To test this theory, an MD was carried out to observe if also low frequency noise can lead to emittance growth and stronger halo population and diffusion. This MD conducted on 24.08.2016 follows a previous MD on 05.11.2015/06.11.2015 [1].

Introduction

To reach the goal of 3000 fb^{-1} integrated luminosity, the HL-LHC upgrade foresees a reduction of β^* to 0.15 m for round collision optics and 0.075/0.30 for flat collision optics, resulting in maximum values of the β-function in the IT of over 20 km and 40 km respectively, compared to RunII LHC optics with 3 km for $\beta^* = 0.80$ m and 6 km for $\beta^* = 0.40$ m. Due to the considerable increase of the β-function in the IT, the HL-LHC becomes more sensitive to any noise introduced by the IT including also ground motion and vibrations. As the power spectral density of ground motion decreases with $1/f$ the amplitudes of the high frequency part of the spectrum become negligibly small and only the low frequency part, approximately up to 100-200 Hz, is relevant. As these frequencies are small compared to the betatron frequencies, the misalignment of the IT by ground motion induces to first order a closed orbit distortion which can be interpreted as low frequency dipole noise.

In various papers [2]–[5] the effect of noise has been analysed and analytical formulas

for the expected emittance growth derived, e.g. [3]:

$$\frac{1}{\epsilon_0}\frac{d\epsilon_x}{dN} = \frac{1-s_0}{4}\left(\Delta^2 + g^2\Delta_{\mathrm{BPM}^2}\right) S\left(\frac{g}{2\pi}|\xi|\right) \tag{1}$$

where N is the turn number, ξ is the tune spread, Δ^2 the noise amplitude (e.g. the dipole kick due to the movement of the IT), Δ^2_{BPM} the noise introduced by the BPMs of the feedback system. $S\left(\frac{g}{2\pi}|\xi|\right)$ describes the effect of the feedback system with gain g and $\frac{1-s_0}{4}$ is a correction factor accounting for the only partial contribution of the coherent beam-beam modes. Similar formulas are derived also in [2], [4], [5], which do not necessarily assume the presence of coherent beam-beam modes. In all cases the expected emittance growth depends on the noise amplitude and tune spread and, more importantly, it is usually assumed that only frequencies close to the betatron sidebands contribute, explicitly the low frequency noise due to ground motion should not result in any emittance growth, increase of tail population or diffusion rate. Furthermore, no emittance growth is expected if the beams are separated.

To investigate if low frequency noise can lead to emittance growth and/or higher tail population a first MD was conducted on 05.11.2015/06.11.2015, fill 4587 to which we will refer in the following as MD2015 [1]. In this MD indications for increased emittance growth due to low frequency noise were found, but as the bunches became unstable during the MD, no definite conclusions could be drawn. Based on the experience during this first MD, a second MD was undertaken on 24.08.2016, fill 5244, to which we will refer as MD2016.

Both MDs have been conducted at injection as the effect of the excitation mainly depends on the tune spread induced by beam-beam, which only depends on the emittance and bunch intensity and is explicitly independent of the energy and β^*. As for high bunch intensities the emittance growth due to intra-beam scattering at injection is expected to be large compared to the emittance growth due to the low frequency excitation [6], [7], a weak-strong scenario has been chosen, so that the effect of the intra-beam scattering can be neglected for the weak beam. For the parameters chosen (2.5 μ m transverse emittance, 1.0 ns bunch length (4 σ), $0.7 \times 10^1 1$ bunch intensity), the emittance growth is around 4.6%/h for the weak bunch. The parameters for the strong beam have been chosen to represent the HL-LHC scenario, where in addition the long-range interactions are mimicked by octupoles. To study the effect of the low frequency excitation, the excitation is switched on and off several times and emittance, transverse beam profiles and beam losses are compared with and without excitation. The low frequency excitation is generated in form of a sinusoidal excitation with the transverse damper (ADT). Besides these equivalent settings, the most relevant differences between the MD2015 and MD2016 are:

- In MD2015 the low frequency excitation was applied on the high intensity bunch and both bunches were not damped with the transverse damper[1]. In MD2016 the

[1]This decision was made as the tail population of the weak bunch, the bunch to be observed, was measured by scraping the beam in several steps with the collimators while observing the beam losses. As the low frequency excitation leads to large orbit distortions, these collimator scans would be perturbed by the excitation if applied on the weak bunch itself and therefore the excitation was applied on the strong bunch.

excitation was instead applied on the weak bunch as no collimator scans were performed in this MD and the strong bunch was damped with the transverse damper.

- In the MD2015 only colliding bunches were used while in the MD2016 colliding and non-colliding bunches were used.
- In MD2016 no collimator scans are conducted in contrast to MD2015.
- Bunches stayed stable in MD2016 while they became unstable in MD2015.
- Chromaticity was increased from $Q'_{x/y} = 3/3$ in MD2015 to $Q'_{x/y} = 7/7$ in MD2016 in order to ensure that the chromaticity stays positive during the entire fill despite eventual drifts and thus no chromaticity induced instabilities occur.

In MD2016 emittance and transverse profiles are measured with the wire scanners and Beam Synchrotron Radiation Telescope (BSRT), and the losses with the Fast Beam Current Transformer (FBCT) and diamond Beam Loss Monitors (dBLM). In this note only the results from the BSRT and FBCT are shown to be followed later by a complete analysis including also the wire scans and dBLM data.

The MD configuration and procedure is described in further detail in Sec. 2 followed by section with some essential checks in Sec. 3. The MD results are summarized in Sec. 5. As the two injections yield very different results despite, there is also a thorough analysis if any changes occurred between the two consecutive injections, which is covered in Sec. 5.4.

MD configuration and MD procedure

In this section we will elaborate the choice of beam parameters, explain the MD configuration and give an overview of the MD procedure.

Choice of beam parameters, chromaticity and octupole current

This section is a summary of the equivalent section in [1]. The aim of this MD is to study the effect of low frequency noise on the beam distribution and therefore all contributing effects need to be included or, if this is not possible, mimicked by other means. First of all, the MD was conducted at injection as experiments are in general more efficient at

Table 1: Estimate of emittance growth due to intra-beam scattering for different beam parameters at injection (E_{beam}=450 GeV), where ϵ_0 is the initial normalized emittance, $\epsilon_{1\text{h}}$ the emittance after one hour and N_b the bunch intensity. The values are given for 1.2 ns bunch length [8].

ϵ_0 [μm]	N_b [10^{11}]	$\epsilon_{1\text{h}}$ [μm]	$(\epsilon_{1\text{h}} - \epsilon_0)/\epsilon_0$ [%]
2.5	2.0	2.68	7.2
	0.8	2.58	3.2
	0.5	2.55	2.0

injection than at top energy and the for this MD relevant effects are independent of the beam energy. Furthermore, as the emittance growth due to noise in general depends on the tune spread (Eqn. 1) and also the non-linearities present, a suited scenario comparable with the HL-LHC needs to be generated at injection. For HL-LHC the strongest sources for the tune spread and non-linearities are the head-on and long-range beam-beam forces. In the MD the head-on interaction are modeled with colliding bunches and the long-range interactions were emulated with octupoles, which are set to ± 6 A (see Fig. 1).

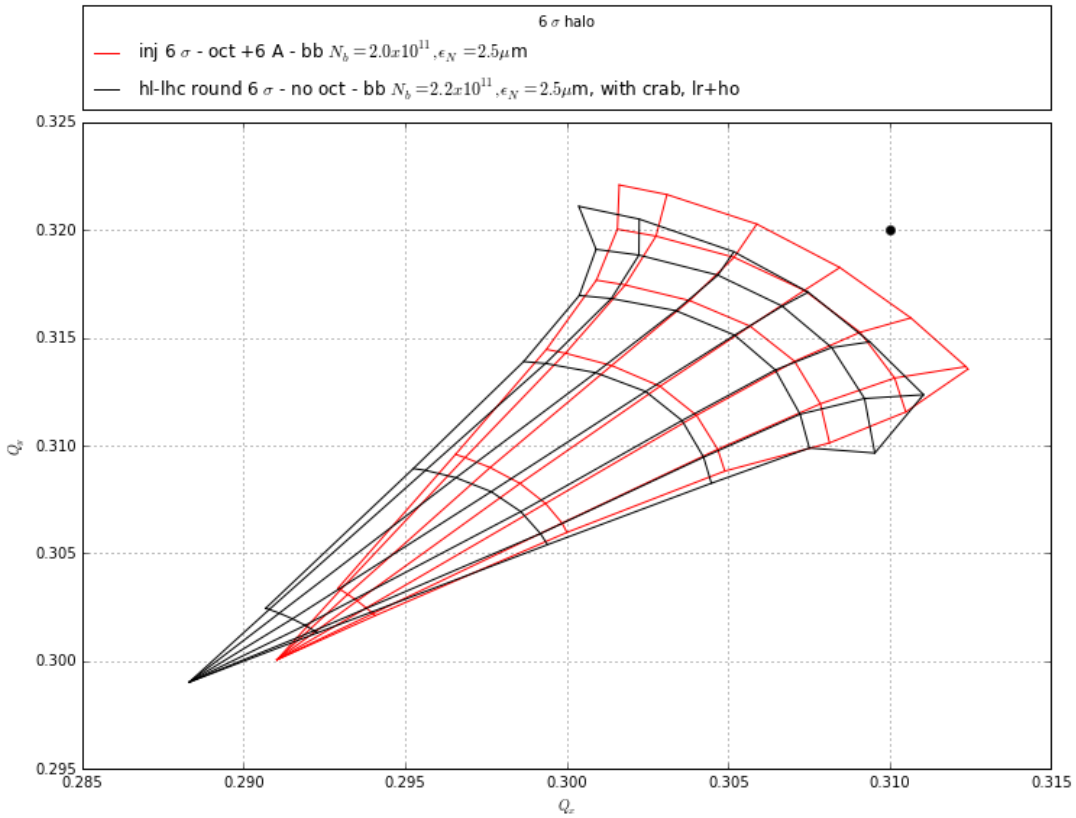

Figure 1: Tune footprint obtained with MAD-X for HL-LHC squeezed optics ($\beta^* = 0.15$ m, half crossing angle ± 295 μm, $N_b = 2.2 \times 10^{11}$, $\epsilon_N = 2.5$ μm, no octupoles) including full crab crossing and the parameters used during the low frequency excitation MD at injection ($\beta^* = 11.00$ m, half crossing angle ± 170 μm, $N_b = 2.0 \times 10^{11}$, $\epsilon_N = 2.5$ μm) using an octupole current of $I_{\mathrm{MOF}} = +6$ A

In order not to be dominated by the emittance growth due to intra-beam scattering at injection and as the emittance growth depends mainly on the tune spread due to beam-beam (neglecting the contribution from coherent beam-beam modes [3]), a weak-strong scenario has been chosen. The same emittance of $\epsilon_N = 2.5$ μm is chosen for the weak and strong bunch in order to avoid any emittance growth due to a mismatch of the beam spot size at the IP [9]. The bunch intensity of the weak beam has been set as low as possible in order to still ensure the correctability of the orbit (the lower limit is about $N_b = 0.5 \times 10^{11}$), explicitly $N_b = 0.7 \times 10^{11}$. Assuming 1.2 ns bunch length (4σ value), the emittance growth due to intra-beam scattering is expected to be around 2-3% per hour for the weak (Beam 2) and 7% for the strong beam (Beam 1), see Table 1. Last but

not least, the bunch intensity of the strong bunch has been lowered to $N_b = 2.0 \times 10^{11}$ in the MD in order to ensure the stability of the bunch [10].

MD configuration

For the MD the following configuration has been chosen:

- injection energy (450 GeV)
- injection optics ($\beta^* = 11$ m), collision tunes, colliding in IP1 and IP5
- bunch intensity of 2.0×10^{11} in Beam 2 and 0.7×10^{11} in Beam 1
- 2.5 μm normalized emittance in Beam 1 and Beam 2
- nominal bunch length of 1.3 ns
- chromaticity of $Q'_{x/y} = 7/7$
- octupole current of $\pm 6A$ (+6A for MOF circuit and -6A for MOD circuit)
- low frequency excitation of Beam 1 with ADT (Beam 2 is not excited)

As the total beam intensity at injection for machine protection reasons is limited to 5.0×10^{11} in case of this MD, only 2 bunches could be injected for the strong beam and in total 6 bunches for the weak beam. The sketch of the filling scheme and the excitation pattern for the weak beam used in this MD is shown in Fig. 2.

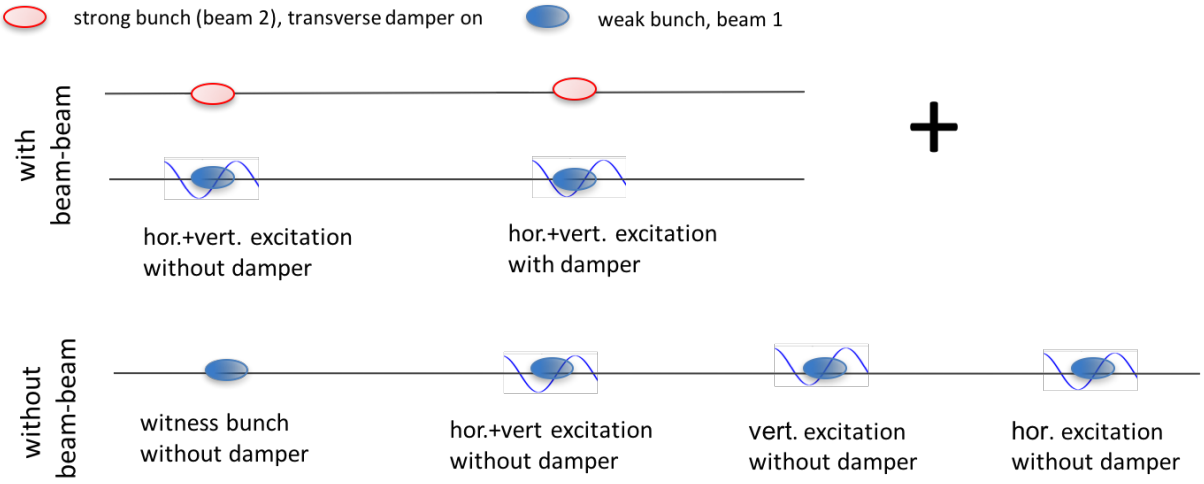

Figure 2: Filling scheme. Bunches of the strong beam (Beam 2) are shown in red and bunches of the weak beam (Beam 1) are shown in blue. The excitation is indicated with a sinus. For the weak beam 2 colliding and 4 non-colliding bunches are used. The strong beam consists of two bunches and the transverse damper is active on both bunches.

The chosen filling scheme aims at answering the following questions:

- Is the effect due to the beam-beam interaction? Thus colliding and non-colliding bunches are compared.
- Is there a sensitivity to the plane of excitation? Thus the excitation is applied in H+V and only in H and only in V.
- Can the effect be mitigated with the transverse damper? Thus bunches with and without transverse damper active are compared.

For the excitation, the same frequencies as in the previous MD (MD2015) have been used, explicitly 11.245 Hz in the horizontal and 22.49 Hz in the vertical plane [1]. These frequencies are close to the first horizontal and vertical eigen-frequencies as measured on the Q1 spare of the current LHC [11] (see Fig. 3).

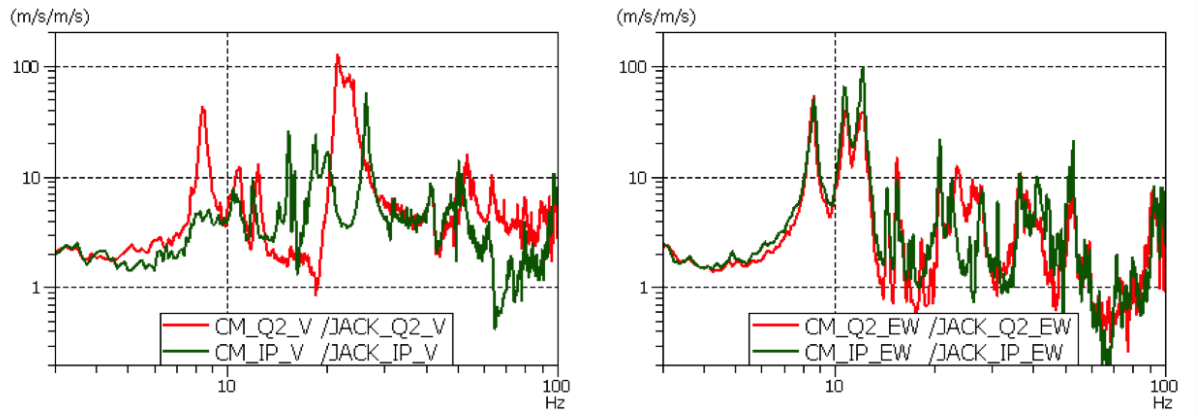

Figure 3: Amplification of noise by the mechanical structure of the Q1. The noise was generated by a drilling machine in SM18 and the horizontal (right) and vertical (left) transfer function from the floor to the cold mass of the Q1 was measured [11]. The first horizontal eigen-frequency is visible at around 8 Hz and the first vertical eigen-frequencies at around 20 Hz. The peak at around 8 Hz in the vertical spectrum is the appearance of the first horizontal eigen-frequency in the vertical spectrum due to coupling of the two planes by the structure. For the first eigen-frequencies an amplification of up to a factor 100 is observed.

MD procedure

This MD was combined with the resonant excitation MD [12]. Prior to both MDs collisions at injection were established using two normal individual bunches per beam. The detailed time line for this MD and the combined resonant excitation MD is described in Table 2. The low frequency noise MD was conducted in fill 5244. The beam was injected two times, referred to in the following as Injection 1 and Injection 2, in order to repeat the experiment at least two times.

Table 2: Time line and list of excitation patterns and amplitudes during this MD and the combined resonant excitation MD [12]. Times are given in Europe/Zurich time. In case of the low frequency excitation the excitation pattern as in Figs. 3 and 6 was always used. A gain of 0.3 corresponds to approximately 0.5 mm peak to peak orbit deviation in the horizontal and vertical plane in the ADT pickups BPMCS.7L4.B1 and BPMCS.7R4.B1 (see Fig. 7).

fill number	time	purpose	excitation
5241	21:14 – 22:37	Establish collisions at injection. After dumping beam of previous MD inject two normal indiv bunches to find collisions.	-
Start resonant excitation MD, see [12].			
5242	22:37 – 23:23	change to injection tunes (0.28/0.31), set octupoles to +19.6 A, set chroma to +15, test resonant excitation with probes	resonant
	23:23 – 02:57	resonant excitation MD, fill 1	
5243	03:11 – 04:08	resonant excitation MD, fill 2	
End resonant excitation MD, see [12].			
5244 Injection 1	04:14 – 05:32	change to collision tunes (0.31/0.32), set octupoles to +6.0 A, set chroma to +7, reestablish collisions at injection with filling scheme as for low frequency noise MD (see Fig. 1), setup ADT	-
Start low frequency noise MD			
	05:32 – 05:58	no excitation (bunch distribution should be fairly adjusted as bunches were already colliding since 05:19)	-
	05:58 – 06:11	start low frequency excitation	low frequency, gain 0.15
	06:11 – 06:39	increase gain to 0.3	low frequency, gain 0.3
5244 Injection 2	06:41 – 07:29	dump and reinject recheck luminosity scans	-
	07:31 – 07:51	no excitation	-
	07:51 – 08:10	low frequency excitation	low frequency, gain 0.3
	08:10 – 08:31	no excitation	-
	08:31 – 08:51	low frequency excitation	low frequency, gain 0.3
End low frequency noise MD			

Cross checks

Stability of tune and chromaticity

Tunes were set to collision tunes of 0.31/0.32 for both beams and kept constant through the entire MD. Chromaticity was kept constant at a value of +7 for both beams. The tunes were measured at the start of Injection 1 (04:28) and rechecked at Injection 2 (06:41). There were no drifts observed. Chromaticity was measured at Injection 1 (04:28) and not remeasured at Injection 2. However, during the previous MD no drifts at all of the chromaticity were observed (see LHC eLogbook) and as the machine stayed the whole day at injection, drifts are very unlikely.

Finding collisions at injection

During the first low frequency noise MD (MD2015, [1]) the bunch was injected in the wrong bucket and it was doubted if collisions were established. In this MD special care was taken to make sure that the beams are colliding in IP1 and IP5 by for example increasing the integration time of the luminosity scans. The luminosity from ATLAS and CMS during fill 5244 is shown in Fig. 4 and the luminosity scans after optimization at Injection 1 and Injection 2 are shown in Fig. 5 showing the parabolic shape expected in case of a successful luminosity scan.

Figure 4: Luminosity during Injection 1 start of Injection 2 of fill 5244. A clear step in luminosity is seen after reoptimization during Injection 1and the values are fully recovered for Injection 2. Note that a first optimization was already done at the end of fill 5242 in preparation of the MD.

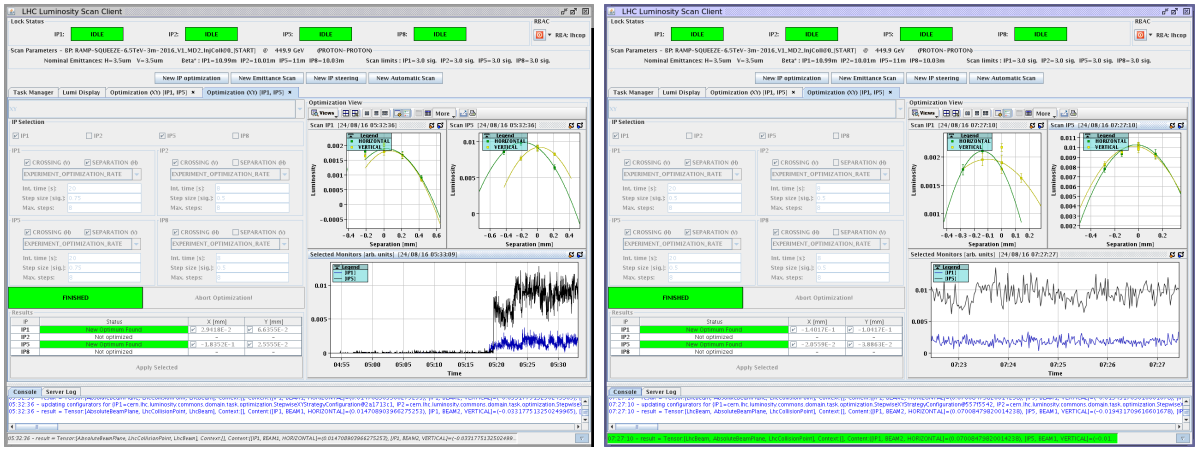

Figure 5: Luminosity scan at the start of Injection 1 at 05:32 (left) and at the start of Injection 2 at 07:27 (right) of fill 5244. In both cases the luminosity scans feature the typical parabolic shape expected in case of a successful luminosity scan.

Low frequency excitation using the transverse damper (ADT)

It is possible to generate a low frequency sinusoidal excitation acting on each beam individually using the transverse damper (ADT), where the maximum kick amplitude of the excitation is given by:

$$x' = (V \times l \times e)/(d \times E_{\text{beam}}) \tag{2}$$

where V is the voltage, e the elementary charge, l the length and d the gap of the ADT kicker and eE_{beam} the beam energy in eV. Assuming ± 7.5 kV per module, 4 kicker modules per beam and plane, a kicker aperture of 52 mm and a length of 1.5 m per module, the kick per module is 0.481 μrad at injection (450 GeV) and 0.033 μrad per module at collision (6.5 TeV). For injection optics and collision tunes this results in the orbit offsets at IP1 and IP5 listed in Table 3.

Table 3: Closed orbit distortion due to an excitation with the maximum ADT kick amplitude (0.481 μrad per module, four modules per beam) at injection ($\beta^* = 11.0$ m) with collision tunes and 2.5 μm normalized emittance. As the optics did not change considerably compared to MD2015, the values are almost the same for both MDs.

	IP	x_{IP} [μm]	y_{IP} [μm]	$\left(\frac{\sigma_x}{x}\right)_{\text{IP}}$	$\left(\frac{\sigma_y}{y}\right)_{\text{IP}}$
Beam 1	1	62.58	61.78	0.26	0.26
	5	-35.73	-10.49	-0.15	-0.04
Beam 2	1	-57.81	-32.56	-0.24	-0.14
	5	3.86	10.28	0.02	0.04

For the excitation, the same frequencies as in the previous MD (MD2015) have been used, explicitly 11.245 Hz in the horizontal and 22.49 Hz in the vertical plane [1]. These frequencies are close to the first horizontal and vertical eigen-frequencies as measured on the Q1 spare of the current LHC [11] (see Fig. 3).

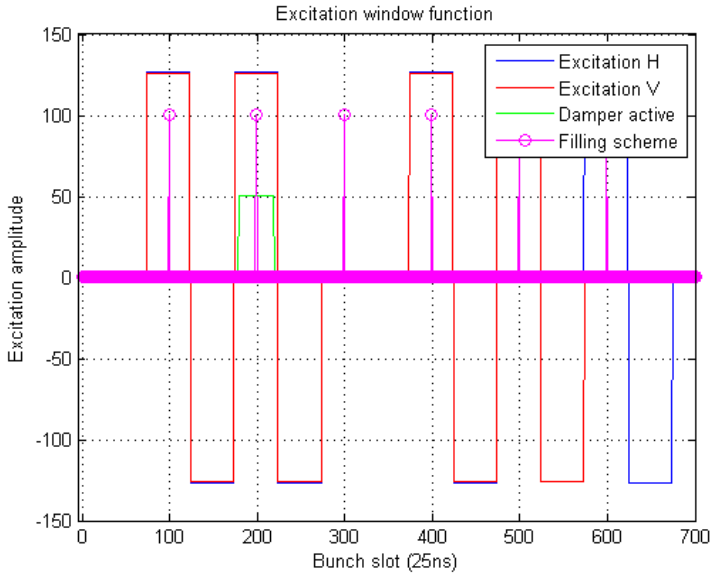

Figure 6: Excitation pattern and gating of the ADT.

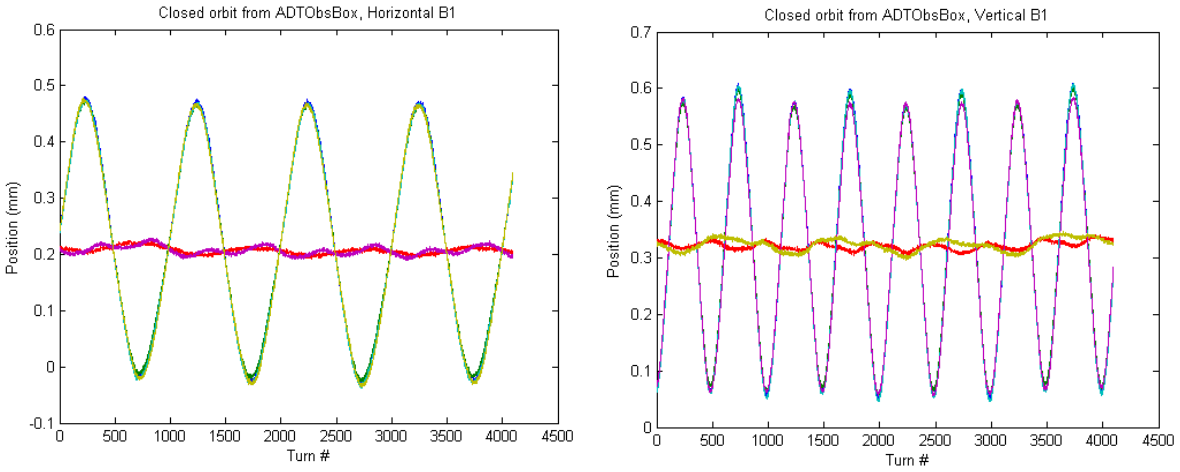

Figure 7: Horizontal (left) and vertical (right) position of the weak beam (Beam 1) as measured with the ADT using BPMCS.7L4.B1 for the horizontal plane and BPMCS.7R4.B1 for the vertical plane[1] and a gain of 0.3. The excitation shows a slightly larger than expected peak-to-peak orbit oscillation of 0.5 mm compared to 0.4 mm assuming a maximum kick amplitude of 0.481 μrad per ADT module (see Table 4).The frequency of the excitation matches perfectly the requested 11.245 Hz in the horizontal and 22.49 Hz in the vertical plane.

In order to test the effect of the low frequency excitation in different beam constellations, the excitation pattern and filling scheme as shown in Fig. 2 was requested. To generate this pattern, the ADT is gated for the weak beam (Beam 1) as shown in Fig. 6. No excitation is applied on the strong bunch (Beam 2) and the transverse damper is kept active during the entire MD in order to ensure that the bunches stay stable.

To verify the excitation shape and amplitude, the orbit was measured with the ADT itself. The closed orbit of the weak beam (Beam 1) at the location of the ADT pick-ups, explicitly BPMCS.7L4.B1 for the horizontal plane and BPMCS.7R4.B1 for the vertical plane [1], is shown in Fig. 7. The frequency of the closed orbit oscillation matches perfectly the requested frequencies of 11.245 Hz in the horizontal and 22.49 Hz in the vertical plane. The peak-to-peak amplitude of the excitation is in both plane approximately 0.5 mm, which is higher than the expected value of 0.4 mm at BPMCS.7[LR]4.B1 assuming 0.481 μrad kick amplitude per module (see Table 4). This implied that most likely a higher maximum kick amplitude of $\frac{0.5 \text{ mm}}{0.4 \text{ mm}} \cdot 0.481$ μrad $= 0.601$ μrad was reached resulting also in slightly larger separation of the beams at the IP (separations in Table 4 must be scaled with $\frac{0.5 \text{ mm}}{0.4 \text{ mm}}$).

Table 4: Closed orbit distortion at the location of the ADT pickups due to an excitation with the maximum ADT kick amplitude of 0.481 μrad per module with in total four modules per beam. Parameters are injection optics ($\beta^* = 11.0$ m) with collision tunes and 2.5 μm normalized emittance. As the optics did not change considerably compared to MD2015, the values are almost the same for both MDs.

ADT pickup	x_{ADT} [mm]	y_{ADT} [mm]
BPMCS.9L4.B1	-0.15	-
BPMCS.7L4.B1	0.21	-
BPMCS.8R4.B1	0.13	-
BPMCS.10R4.B1	-0.23	-
BPMCS.10L4.B1	-	-0.23
BPMCS.8L4.B1	-	0.16
BPMCS.7R4.B1	-	0.20
BPMCS.9R4.B1	-	-0.10

BSRT emittance and BSRT profiles at injection

This chapter intends to give a short overview of the BSRT profile analysis presented in this note and the general beam profiles at injection. For a more detailed description of the analysis, it is referred to [14] and a detailed description of the BSRT can be found in [15]. The BSRT image formation is mathematically described as a convolution of the beam distribution with the optical resolution (LSF). Assuming that the beam distribution

[1]The ADT is equipped with in total 4 pickups [13]. During the MD we did not note down which pick-up was used. However, the pick-ups BPMCS.10[LR]4.B1 were not connected and we had files saved only for BPMCS.7[LR]4.B1, so we are confident that for the plots shown in Fig. 7 the pickpus BPMCS.7[LR]4.B1 were used.

as well as the optical resolution (LSF) are Gaussian, a conversion factor $c_{\mathrm{LSF},z}$ ("LSF factor") can be derived, which is defined as the the width of the Gaussian distribution of the optical resolution[1]. The sigma $\sigma_{\mathrm{profile}}$ of the BSRT profile can then be converted to beam sigma σ_{beam} by:

$$\sigma_{\mathrm{beam},z} = \sqrt{\sigma^2_{\mathrm{profile},z} - c^2_{\mathrm{LSF},z}},\ z = h, v. \tag{3}$$

The position can then be very roughly also be expressed in beam sigma:

$$z[\sigma_{\mathrm{beam},z}] = \frac{z[\mathrm{mm}]}{\sigma_{\mathrm{beam},z}[\mathrm{mm}]},\ z = h, v. \tag{4}$$

Using the β-function at the location of the BSRT and assuming no coupling between the transverse planes, the emittance is then given by:

$$\epsilon_{\mathrm{beam},z} = \frac{\sigma^2_{\mathrm{beam},z}}{\beta_{\mathrm{BSRT},z}},\ z = h, v. \tag{5}$$

The LSF factor $c_{\mathrm{LSF},z}$ as well as the β-function at the location of the BSRT are logged in the LHC Logging database together with the sigma of the BSRT profiles $\sigma_{\mathrm{profile}}$. The full profiles are not logged by default and need to be saved using a special application.

The BSRT profiles are in general a projection of the BSRT synchrotron light black and white image projected on the horizontal and vertical axis. The result are histograms in both planes representing the projections of the horizontal/vertical bunch distribution. The BSRT can take images of only one bunch at a time and in order to record all bunches during one fill the device loops through the individual bunches. For each time stamp several profiles of the same individual bunch are taken. In this MD, explicitly three profiles of one individual bunch were taken for each time stamp (see profile 1–3 in green and blue in Fig. 8). Using these profiles, the general steps in the analysis are:

1. The profiles are converted to probability distributions $\rho(x)$ by dividing the bin height by the integral over the profile, so that:

$$\int_{-\infty}^{\infty} \rho(x) = 1 \tag{6}$$

2. The background is calculated by averaging the first and last ten bins of all profiles for each individual bunch over the complete time of acquisition. This constant is then subtracted from the normalized distribution. After the background subtraction, the profiles are renormalized so that the integral over the distribution is one. The profiles are checked before and after background subtraction, as this can hide real physical effects or also introduce artificial features.

3. The profiles are averaged in order to reduce the noise. Explicitly the profiles are averaged in two different ways:

[1]The convolution of two uni-variate Gaussian distributions f and g having respectively the means μ_f and μ_g and standard deviation σ_f and σ_g is a Gaussian distribution with mean and standard deviation $\mu_{f*g} = \mu_f + \mu_g$ and $\sigma_{f*g} = \sqrt{\sigma_f^2 + \sigma_g^2}$

- the three profiles of each individual bunch are averaged for each time stamp ("average profile"). The average profile is then fitted with a Gaussian and q-Gaussian distribution.
- the moving average and standard deviation over 11 time stamps ("moving average profile") is taken. Thus with three profiles per time stamp in total 33 profiles are averaged. The obtained standard deviation for each bin is used as an estimate for the error in each bin. These estimated errors are then used as weights for the least square fit of the Gaussian and q-Gaussian distribution and for the calculation of the chi-squared as a measure of the goodness of the fit. The moving average profile is shown as a black line in Fig. 8. Note that in case of a low frequency excitation the moving average of the profiles should not be used as the centroid of the profiles shifts from one time stamp to the next and the profiles are thus not centered at the same position. The centroid is in general not subtracted from the profiles as no robust estimate of the centroid could be obtained.

4. A Gaussian (light red dashed line in Fig. 8) and q-Gaussian distribution (dark red line in Fig. 8) are fitted to the average profile and the moving average profile. In case of the moving average profile, the fit is weighted with the calculated standard deviation for each bin.

   The Gaussian distribution is defined as

$$f_{\text{Gauss}}(x) := c + a \cdot \frac{e^{-\frac{(x-\mu)^2}{2\sigma^2}}}{\sqrt{2\pi}\sigma}, \tag{7}$$

   where μ is the mean and σ the standard deviation of the distribution.

   The q-Gaussian distribution is defined as

$$f_{\text{q-Gauss}}(x) = c + a \cdot \frac{\sqrt{\beta}}{C_q} e_q(-\beta(x-\mu)^2), \tag{8}$$

   where μ is the mean of the distribution and

$$e_q(x) = (1 + (1-q)x)^{\frac{1}{1-q}} \tag{9}$$

   is the q-exponential. The normalization factor C_q is given by

$$C_q = \frac{\sqrt{\pi} \cdot \Gamma\left(\frac{3-q}{2(q-1)}\right)}{\sqrt{q-1} \cdot \Gamma\left(\frac{1}{q-1}\right)}, \text{ for } 1 < q < 3, \tag{10}$$

   For $q < \frac{5}{3}$ the standard deviation σ is then given by:

$$\sigma^2 = \frac{1}{\beta(5-3q)} \tag{11}$$

   For other values of q the standard deviation is either infinite or not defined. The range of the parameter q is limited to $0 < q < 3$. The parameter q is an estimator

for the tail population. For $q \to 1$ the Gaussian distribution is recovered, for $q > 1$ the distribution features heavier tails compared to the Gaussian distribution and for $q < 1$ lighter tails. The parameter c is introduced in the Gaussian and q-Gaussian fit in order to model the background of the profiles implying the introduction of the parameter a in order to fulfill the requirement that the integral over the distribution is one.

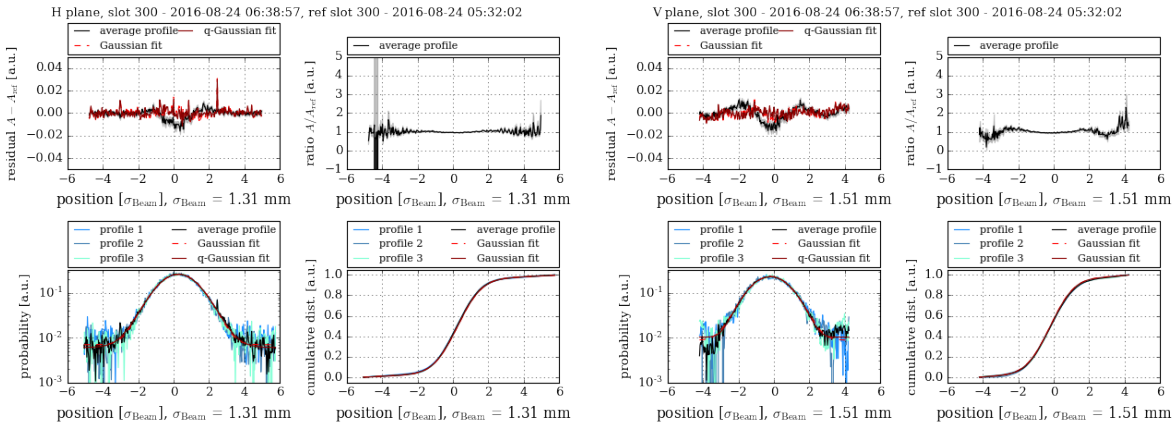

Figure 8: Typical BSRT profile at injection for the horizontal (left) and vertical (right) plane. The profile was taken just before the low frequency excitation is switched on in Injection 1 of fill 5244 (2016-08-24 06:38:57) and for a bunch not experiencing any excitation and also with the transverse damper not active. The residual and ratio are taken in respect to a profile at the beginning of the fill (2016-08-24 05:32:02). The background is not subtracted and the moving average profiles are shown as black line in all subplots. For the moving average the profiles are explicitly averaged over 11 time stamps with 3 profiles per time stamp. Note that the x-axis is the position of the BSRT image projection in units of the σ from the Gaussian fit of the profile and *not* the proton beam sigma. The raw profiles for this time stamp are shown in blue and green in the probability distribution (lower left) and cumulative sum (lower right). For the residual and ratio, the moving average profile is shown in black together with the 1σ standard deviation over the 11 time stamps as gray envelope. The Gaussian fit is shown in dashed red and the q-Gaussian fit in solid dark red in the profile plot (lower left) and the deviation from the fit with the same color coding in the residual plot (upper left).

5. statistical parameters are calculated for the average and moving average profile, including the cumulative sum of the distribution shown in Fig. 8 lower right.

6. To better visualize the changes of the distribution, the residual Res and the ratio Rat for bunch i at time stamp t_i in respect to reference bunch j at time stamp t_j are calculated with

$$\mathrm{Res}(t_i, x) = A_i(t_i, x) - A_j(t_j, x) \tag{12}$$

$$\mathrm{Rat}(t_i, x) = \frac{A_i(t_i, x)}{A_j(t_j, x)} \tag{13}$$

where $A_i(t_j, x)$ denotes the amplitude at bin x of bunch i at time stamp t_j. In this MD the residual and ratio are taken in respect to the initial distribution of the bunch itself, explicitly:

$$\mathrm{Res}(t_i, x) = A_i(t_i, x) - A_i(t_j, x) \tag{14}$$

$$\mathrm{Rat}(t_i, x) = \frac{A_i(t_i, x)}{A_i(t_j, x)} \tag{15}$$

The residual is in general sensitive to changes in the core region and the ratio to changes in the tails. The residual proved to be a good indicator for changes in the core while the ratio turned out to be too sensitive to the noise of the BSRT profiles.

A typical bunch distribution for a reference bunch without any excitation is shown in Fig. 8 and the q-parameters for all bunches during the time without excitation is shown in Fig. 9 for Injection 1 and in Fig. 26 for Injection 2. Both injection show a similar behavior of the q-Parameter. The following observations can be maid:

- The distribution in the *horizontal* plane features slightly over-populated tails for Beam 1 (weak beam) and the q-Gaussian fit represents a better model for the distribution. The tails are slowly depleted during the fill as illustrated in Fig. 9 showing a decrease of q starting from $q \approx 1.25 - 1.15$ for all bunches. Furthermore, the bunches without collisions feature a higher tail population than the bunches with collisions. For Beam 2 (strong beam) the beam tails are almost perfectly Gaussian ($q \approx 1$).

- The distribution in the *vertical* plane has slightly underpopulated tails as $q \approx 0.95 < 1$ (see Fig. 9). The q-parameter stays unchanged for Beam 1 (weak beam) and decreases for Beam 2 (strong beam).

- The distribution shows a "bump" on the right side (positive position) of the horizontal profile and left side (negative positions) of the vertical profile. A possible explanation for the bump could be a spot in the image. Note that the bump is not well visible in Fig. 8.

- There are strong oscillations of the distribution during the fill mostly visible as fluctuation in the residual of the distribution. By averaging over several profiles as done in the moving average, the fluctuations can be reduced.

- The cumulative sum (CDF) of the distribution is a smooth function for both planes and can be used to define a model independent definition of the standard deviation σ of the distribution [1]. Based on the analogy of the cumulative distribution function and the standard deviation for a Gaussian distribution we define the standard deviation σ as:

$$\sigma_{32} = \mathrm{CDF}^{-1}(0.32) \tag{16}$$

$$\sigma_{68} = \mathrm{CDF}^{-1}(0.68) \tag{17}$$

[1] The BSRT emittance obtained from the LHC logging database (see Sec. **??**) is the sigma of the distribution obtained via a Gaussian fit to the distribution assuming that a Gaussian fit is a well suited model. For example in the horizontal plane the tails are over-populated and the Gaussian distribution does not represent a good model.

The left and right side are calculated separately because of the bumps in the BSRT distribution on the left for the vertical and right for the horizontal.

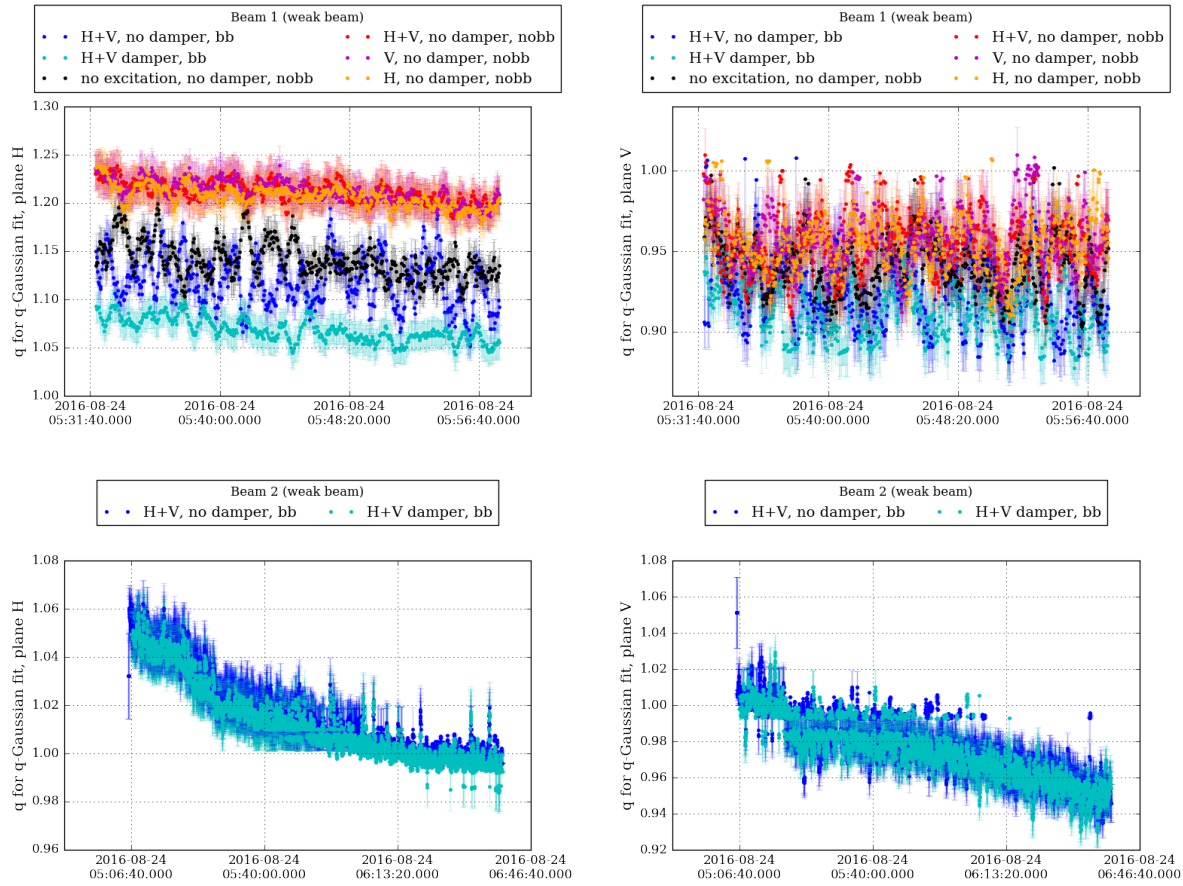

Figure 9: q parameter of q-Gaussian fit in the horizontal (left) and vertical (right) plane: q-parameter without excitation during Injection 1 in fill 5244 for Beam 1 and during the entire Injection 2 for Beam 2. Beam 1 (weak beam) is shown on the top and and Beam 2 (strong beam) is shown on the bottom. The bunches of Beam 2 are both colliding and are labeled according to their partners in Beam 1. For Beam 2 no excitation is applied and the transverse damper is active for both bunches. The q-Gaussian fit is performed for the average profiles and without background subtraction. The errorbars contain only the error from the q-Gaussian fit obtained from the covariance matrix ($\sigma_q = \sqrt{(\mathrm{cov}(p_q, p_q)}$ where p_q indicates the diagonal element of the matrix for the fit parameter q).

MD results

To evaluate the effect of a low frequency excitation, the excitation was switched on and off and the emittance, bunch length, beam losses and transverse beam profiles are compared for the case with and without excitation. During Injection 1 the excitation was switched on/off only once and during Injection 2 the excitation was switched on/off twice (see Table 2). First a few plots of the bunch intensity, emittance and bunch length during the

entire fill are summarized in Sec. 5.1 in order to give an overview of the beam parameters during the two fills. Then the results from the beam losses as measured with the Fast Beam Current Transformers (FBCT) and the emittance as measured with the Beam Synchrotron Radiation Telescope (BSRT) and as saved in the LHC Logging database are summarized in Sec. 5.2 for Injection 1 and Sec. 5.3 for Injection 2 respectively. This analysis yields different results for the two injections. In Sec. 5.4 an attempt is made to find out the reason for the different results for the two injections, however with limited success.

Beam parameters during the entire fill 5244

The bunch intensity measured with the Fast Beam Current Transformer (FBCT), the bunch length from the Beam Quality Monitor (BQM) and the emittance measured with the Beam Synchrotron Radiation Telescope (BSRT) are shown in Fig. 10–12. The bunches stayed stable during the entire fill. For both beams the emittances were larger than requested, explicitly between $2.5 - 3.5$ μm instead of 2.5 μm. Slightly smaller emittances were achieved for the weak beam during the second injection. The achieved bunch intensity were as requested, explicitly around 0.7×10^{11} for the weak beam and around 2.0×10^{11} for the strong beam.

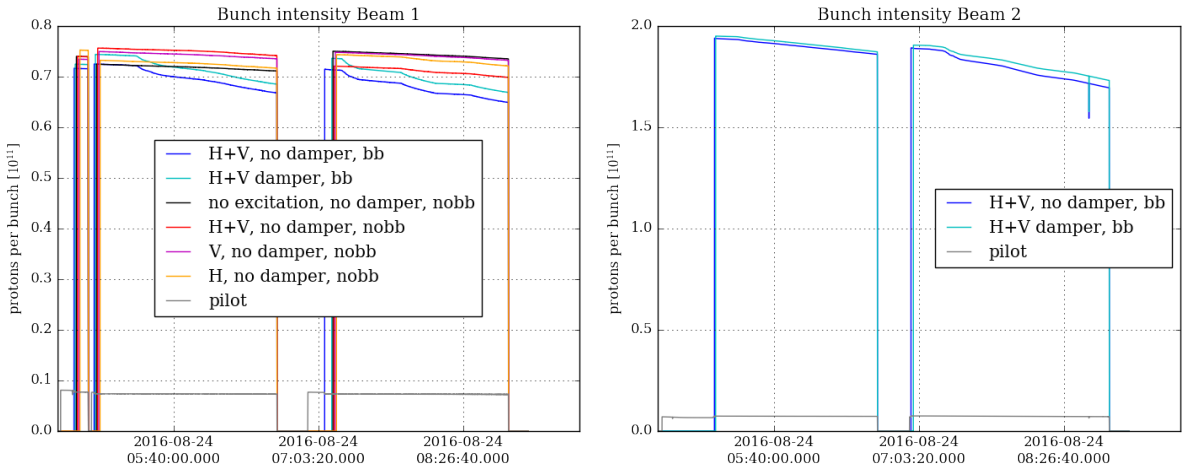

Figure 10: Bunch intensity measured with the FBCT, explicitly LHC.BCTFR.A6R4.B[12]:BUNCH_INTENSITY, for the weak beam (left) and the strong beam (right). The strong beam is labeled according to the colliding bunches of the weak beam. For the strong beam (Beam 2) no excitation is applied and the damper is active during the entire fill.

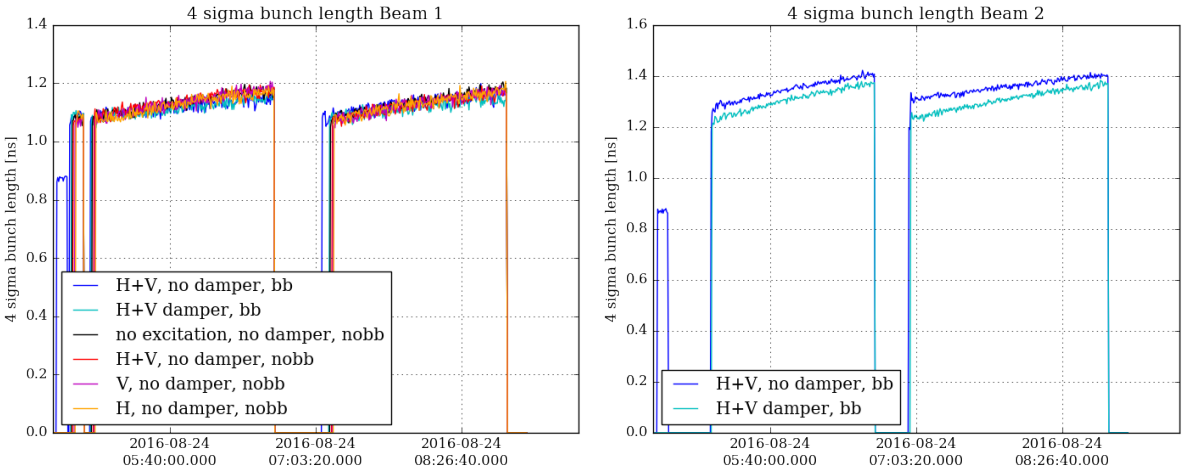

Figure 11: Bunch length from the BQM, explicitly LHC.BQM.B[12]:BUNCH_LENGTHS, for the weak beam (left) and the strong beam (right). The strong beam is labeled according to the colliding bunches of the weak beam. For the strong beam (Beam 2) no excitation is applied and the damper is active during the entire fill.

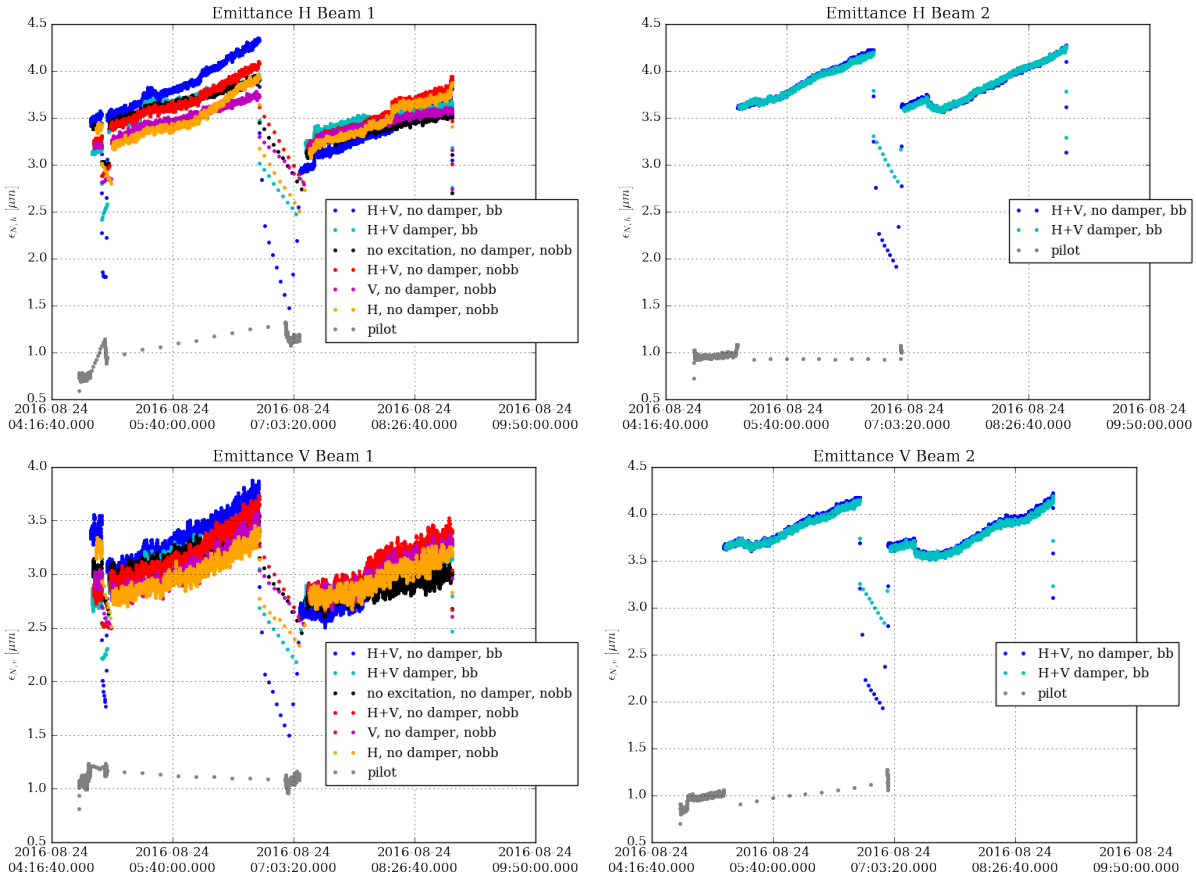

Figure 12: Emittance as measured with the BSRT for the weak beam (left) and the strong beam (right). The strong beam is labeled according to the colliding bunches of the weak beam. For the strong beam (Beam 2) no excitation is applied and the damper is active during the entire fill.

Injection 1

The bunch by bunch relative beam losses as measured with the FBCT and the emittance as measured with the BSRT are shown in Fig. 13–14. The following observations can be made:

- No change of the beam losses is observed due to the low frequency excitation.
- For non-colliding bunches a clear increase of the horizontal emittance growth is observed for a low frequency excitation in H+V and only in H. No change of the vertical emittance growth due to the low frequency excitation is visible. For colliding bunches, the horizontal emittance growth increases with a low frequency excitation in H+V without damper. With damper, the emittance growth increase disappears.

In summary, a low frequency excitation in the horizontal plane (or horizontal and vertical) apparently leads to emittance growth for colliding and non-colliding bunches. This emittance growth can be mitigated with the transverse damper.

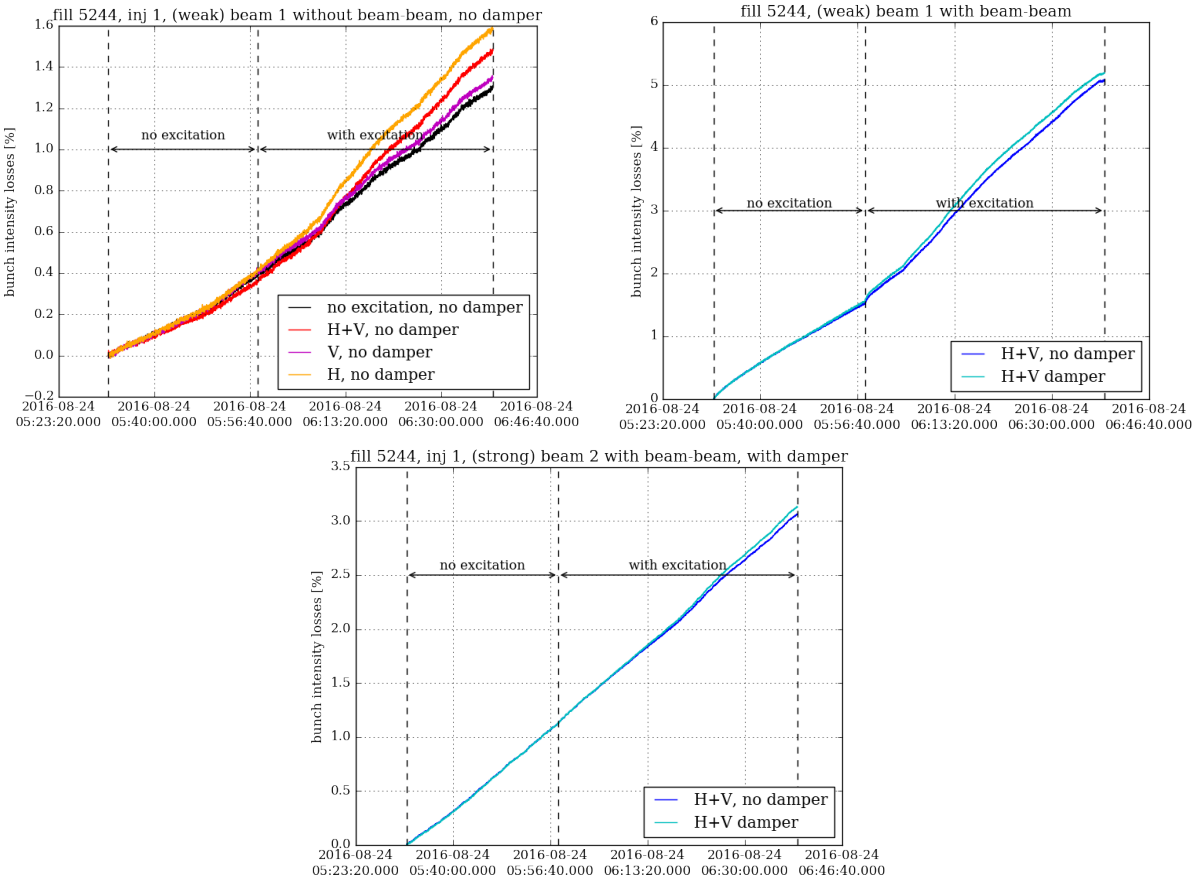

Figure 13: Injection 1: Bunch intensity measured with the FBCT for the weak beam (top) and the strong beam (bottom). The bunches of the weak beam are split up in two plots, where the non-colliding bunches are shown on the top left and the colliding bunches on the top right. The strong beam is labeled according to the colliding bunches of the weak beam. For the strong beam (Beam 2) no excitation is applied and the damper is active during the entire fill.

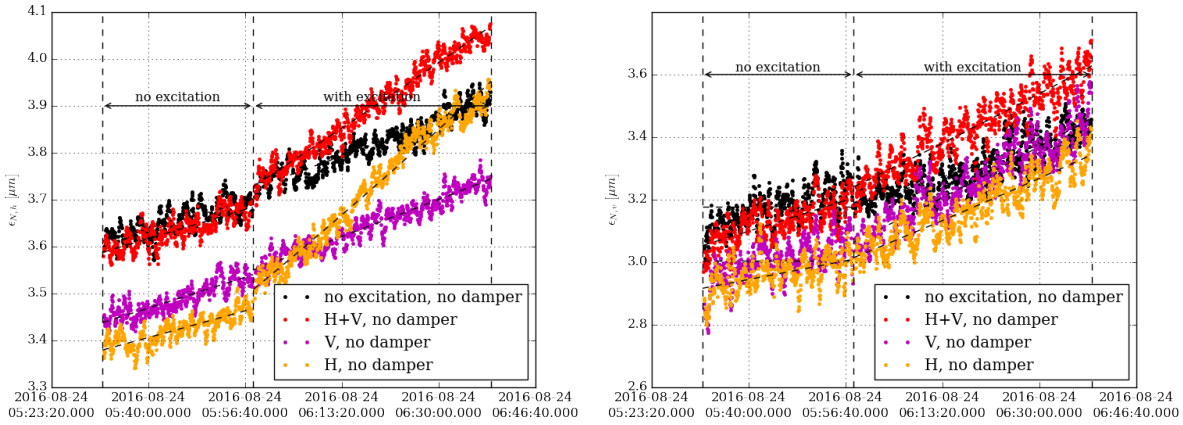

Figure 14: Injection 1: Horizontal (left) and vertical (right) beam emittance measured with the BSRT for the non-colliding bunches of the weak beam. A clear increase of the horizontal emittance in case of an excitation in H and in H+V is visible.

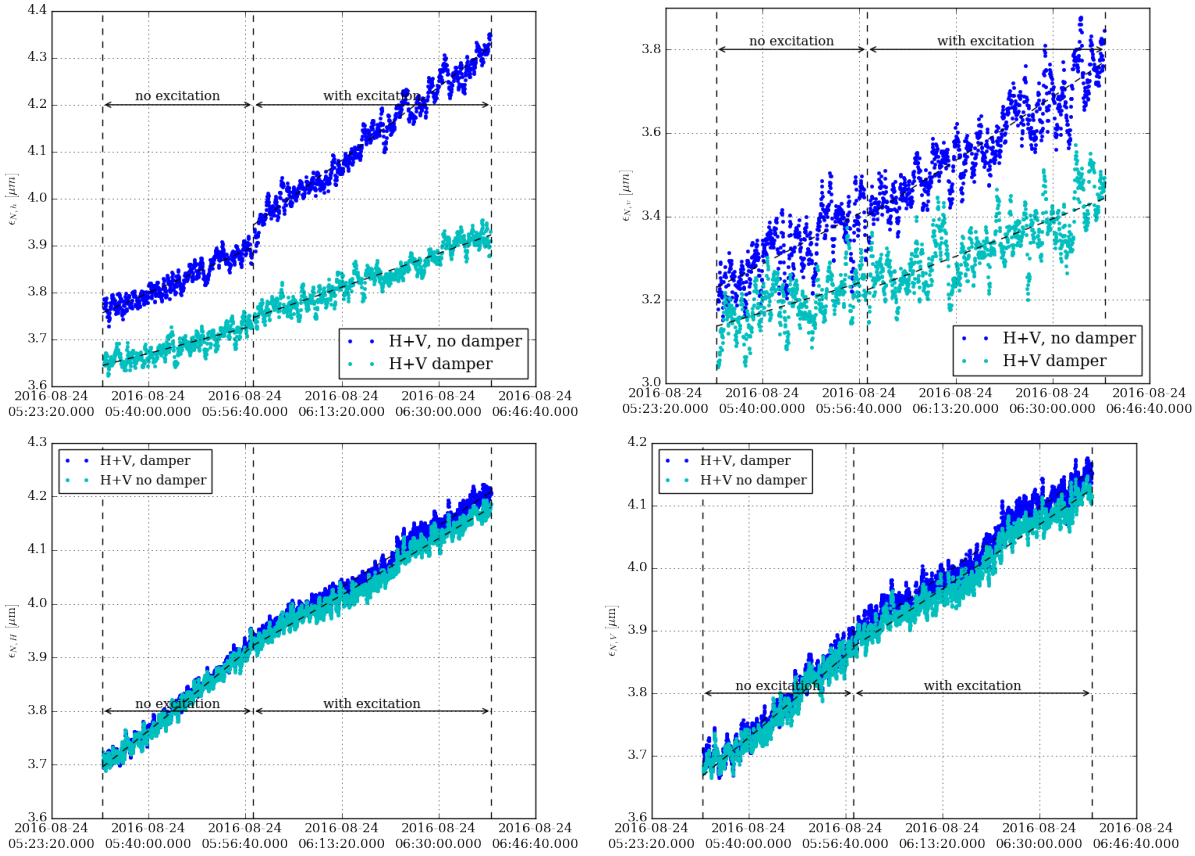

Figure 15: Injection 1: Horizontal (left) and vertical (right) beam emittance measured with the BSRT for the colliding bunches of the weak beam (top) and strong beam (bottom). The strong beam is labeled according to the colliding bunches of the weak beam. For the strong beam (Beam 2) no excitation is applied and the damper is active during the entire fill. A clear increase of the horizontal emittance in case of an excitation in H and in H+V is visible.

Injection 2

The bunch by bunch relative beam losses as measured with the FBCT and the emittance as measured with the BSRT are shown in Fig. 16–17. The following observations can be made:

- In case of a low frequency excitation in H+V and only in H a clear increase of the relative beam losses of the weak beam is observed. This is the case for colliding (here only H+V was tried) and non-colliding bunches and with and without transverse damper active. No change in case of an excitation only in V is visible. However in contrast to the emittance growth during Injection 1 the losses can not be mitigated with the transverse damper.
- A change of the emittance is visible when the low frequency excitation is switched on and off. This emittance change is however a convolution of the (possible) beam distribution change due to the low frequency excitation and the beam losses. As it is not possible to disentangle both effects, a conclusion is not possible.

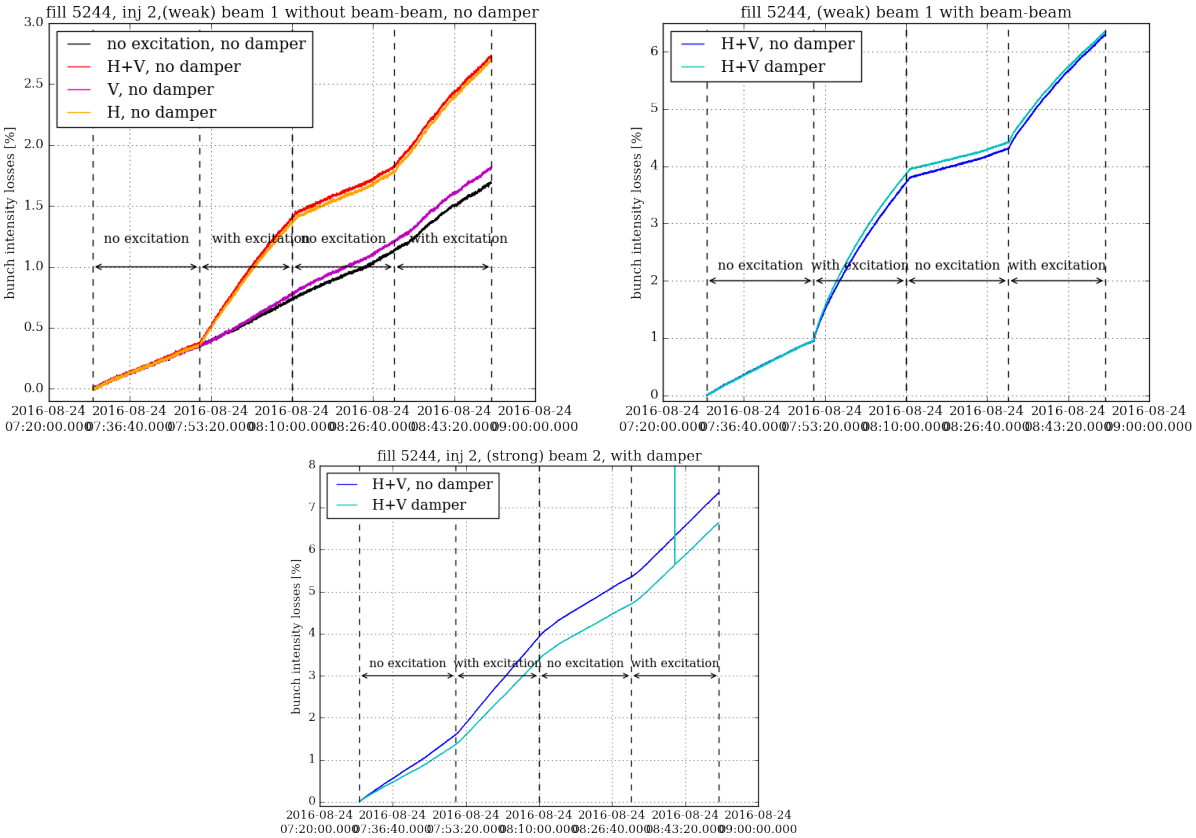

Figure 16: Injection 2: Bunch intensity measured with the FBCT for the weak beam (top) and the strong beam (bottom). The bunches of the weak beam are split up in two plots, where the non-colliding bunches are shown on the top left and the colliding bunches on the top right. The strong beam is labeled according to the colliding bunches of the weak beam. For the strong beam (Beam 2) no excitation is applied and the damper is active during the entire fill.

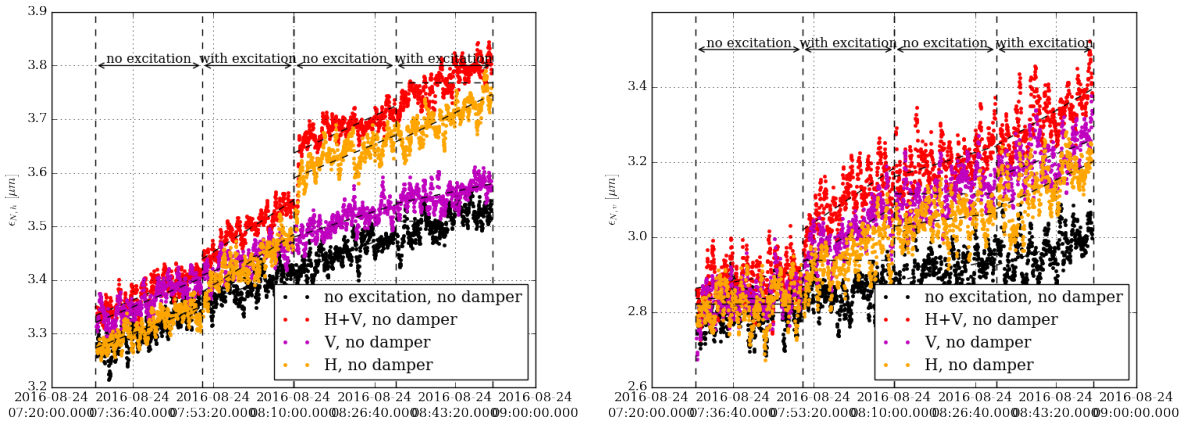

Figure 17: Injection 2: Horizontal (left) and vertical (right) beam emittance measured with the BSRT for the non-colliding bunches of the weak beam. A clear increase of the horizontal emittance in case of an excitation in H and in H+V is visible.

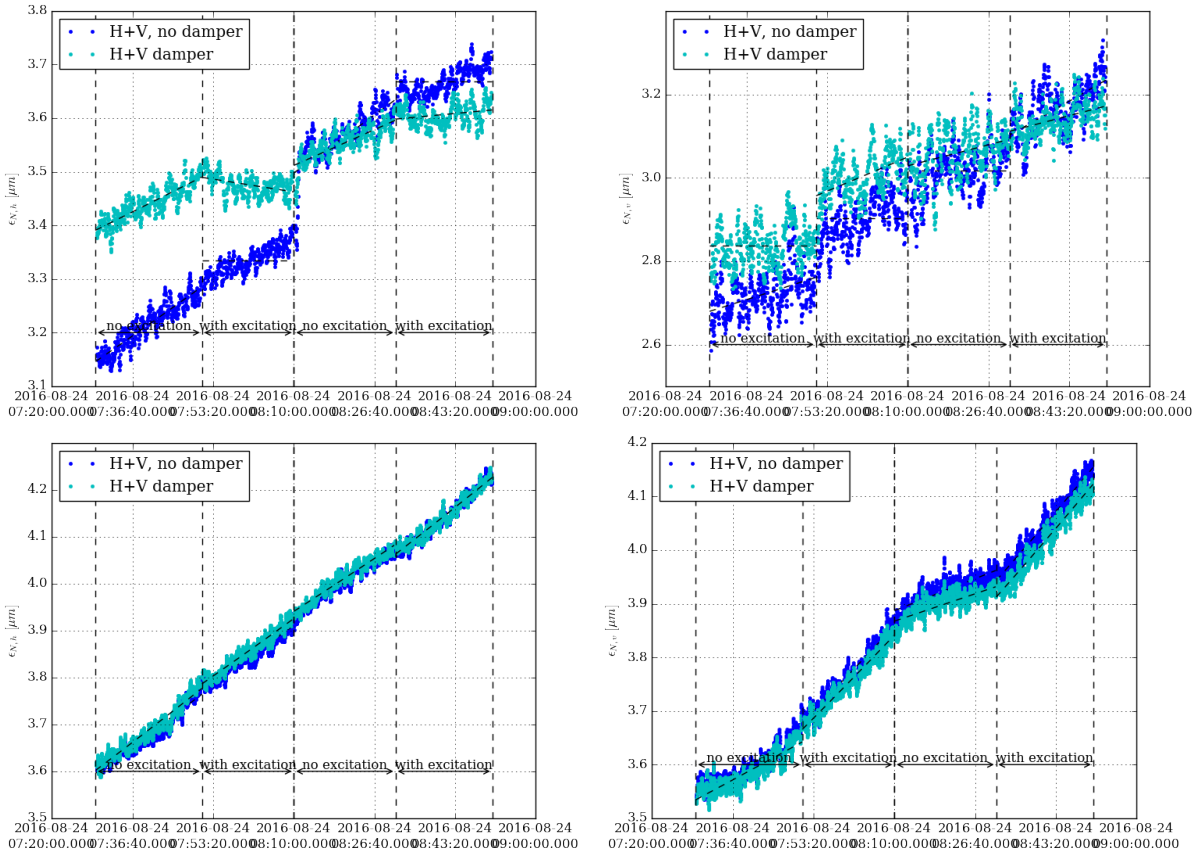

Figure 18: Injection 2: Horizontal (left) and vertical (right) beam emittance measured with the BSRT for the colliding bunches of the weak beam (top) and strong beam (bottom). The strong beam is labeled according to the colliding bunches of the weak beam. For the strong beam (Beam 2) no excitation is applied and the damper is active during the entire fill. A clear increase of the horizontal emittance in case of an excitation in H and in H+V is visible.

In summary, a low frequency excitation in the horizontal plane (or horizontal and vertical) apparently leads to beam losses for colliding and non-colliding bunches. These beam losses can not be mitigated with the transverse damper. No conclusion can be drawn concerning the emittance growth.

Analysis of Orbit drifts, BLM signals, injection oscillations and BSRT profiles

Orbit drifts at TCPs

The beam position during the entire fill as measured with the BPMs closest to the TCPs in the betatron collimation in IR7 and the momentum collimation in IR3 is shown in Fig. 19. For IR7 the 4 BPMs closest to the TCPs are shown and for IR3 only the 2

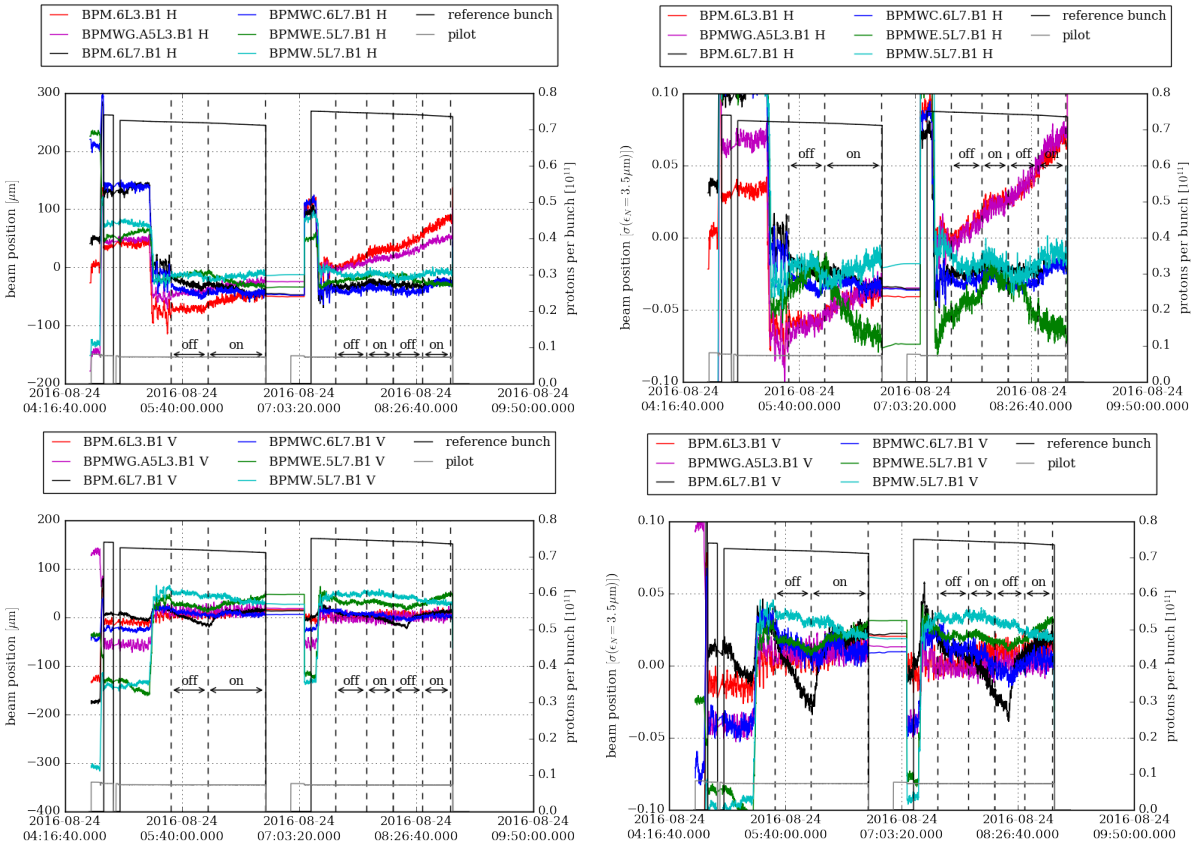

Figure 19: Beam position of Beam 1 (weak beam) as measured with the BPMs closest to the TCPs. To show better the relative changes, the mean position during the fill is subtracted from the beam position. Explicitly, $z - z_{\text{mean,fill}}$ is shown, where z is the beam position as measured with the BPMs. The right plot is a zoom of the left plot with the beam position expressed in beam sigma at the location of the BPM and for an emittance of 3.5 μm as used for the collimator settings. The beam intensity measured with the FBCT of Beam 1 of the pilot and reference bunch are shown in addition in black and gray. The switching on/off of the low frequency excitation is indicated with "on" and "off".

closest ones. The large orbit excursion in the beginning are due to the luminosity scans. During the actual measurements the orbit changes stay below 0.05 σ at the locations of the TCPs in IR7 and below 0.2 σ at the location of the TCPs in IR3. Note that only at the TCPs in IR7 the increased losses during the low frequency excitation are observed, so the larger orbit drifts at the TCPs in IR3 cannot explain the difference between the two injections (see Sec. 5.4.2).

Beam losses close to TCPs as measured with adjacent BLMs

The beam losses measured with the BLMs closest to the TCPs and for an integration time of 1.31072 s (Running sum RS09) are shown in Fig. 20. The measured data with the BLMs confirms the FBCT data in terms of that a small or no increases of losses with a low frequency excitation is observed for Injection 1 and a strong increase is observed for Injection 2.

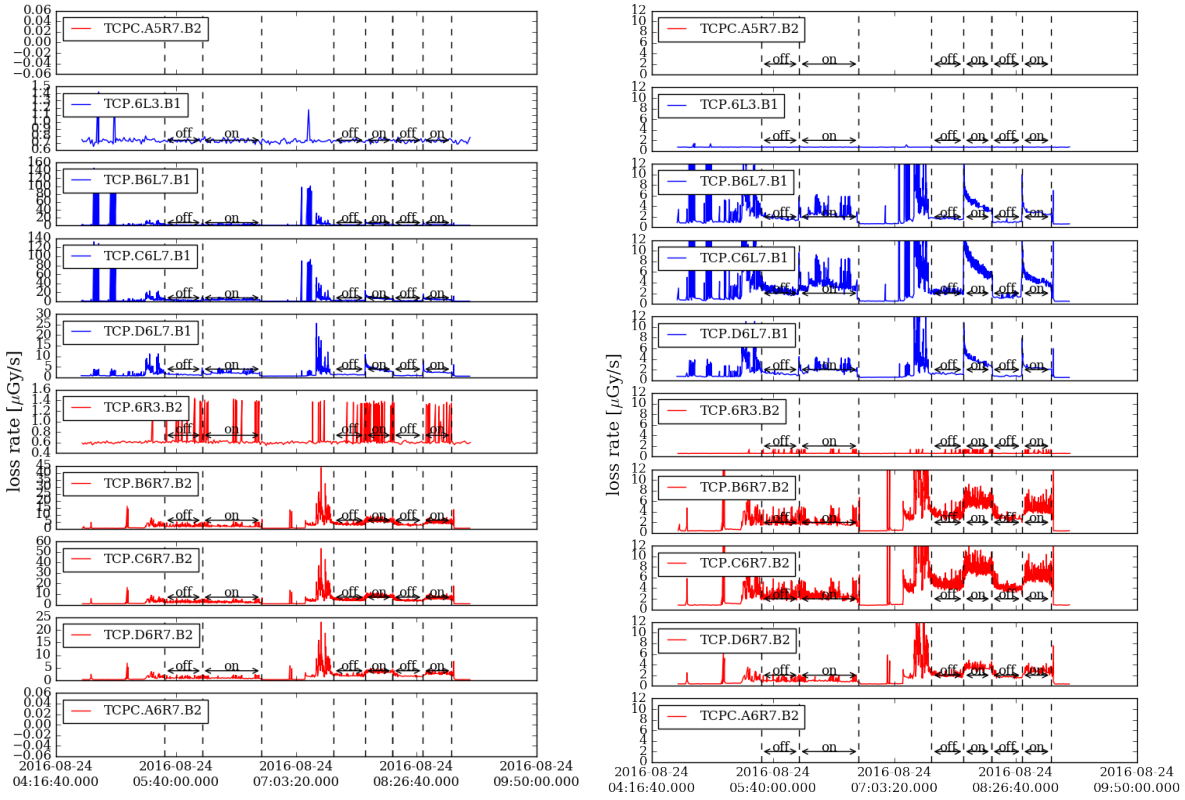

Figure 20: Losses as measured with the BLMs closest to the TCPs for an integration time of 1.31072 s (Running sum RS09). The right plot is simply a zoom of the y-axis of the left plot.

In more detail, the BLM data reveals:

Injection 1: The BLM signal does not feature the typical exponential decay for a scraping of the beam distribution with the TCPs. Instead the loss level of Beam 1 (weak beam) is slightly increased with also some loss spikes while the low frequency excitation is applied. For Beam 2 (strong beam) there is no change in the loss rate.

Injection 2: A step like increase of the losses followed by an exponential decay indicates that the beam is scraped by the TCPs due to the orbit movement induced by the low frequency excitation. A slightly elevated loss level during the low frequency excitation is also observed for Beam 2 (strong beam) which is coupled through the beam-beam interaction with the excited Beam 1 (weak beam). The increase of the losses can be either due to the offset collisions at the IP and thus stronger non-linearities or simply due to the transfer of the orbit movement due to the low frequency from Beam 1 (weak beam) to Beam 2 (strong beam).

Location of losses: The increase of losses is only seen in the BLMs close to the TCPs in IR7, but not for the ones close to the TCPs in IR3.

Injection Oscillations

A possible source of a change of the tail population can be a difference in the injection oscillation. The first 4096 turns after the injection of each bunch are recorded with the ADT (variable ADT[HV].SR4.M1.B1:FIXDISPLAY_Q[79]). These injection oscillations over the first 300 turns are shown in Fig. 21. Injection 1 and Injection 2 of all 7 bunches (6 bunches + 1 pilot) of Beam 1 (weak beam) measured with the ADT pick-up at Q7 and Q9 are shown in red and green in Fig. 21–22 with an almost perfect agreement of the two injections.

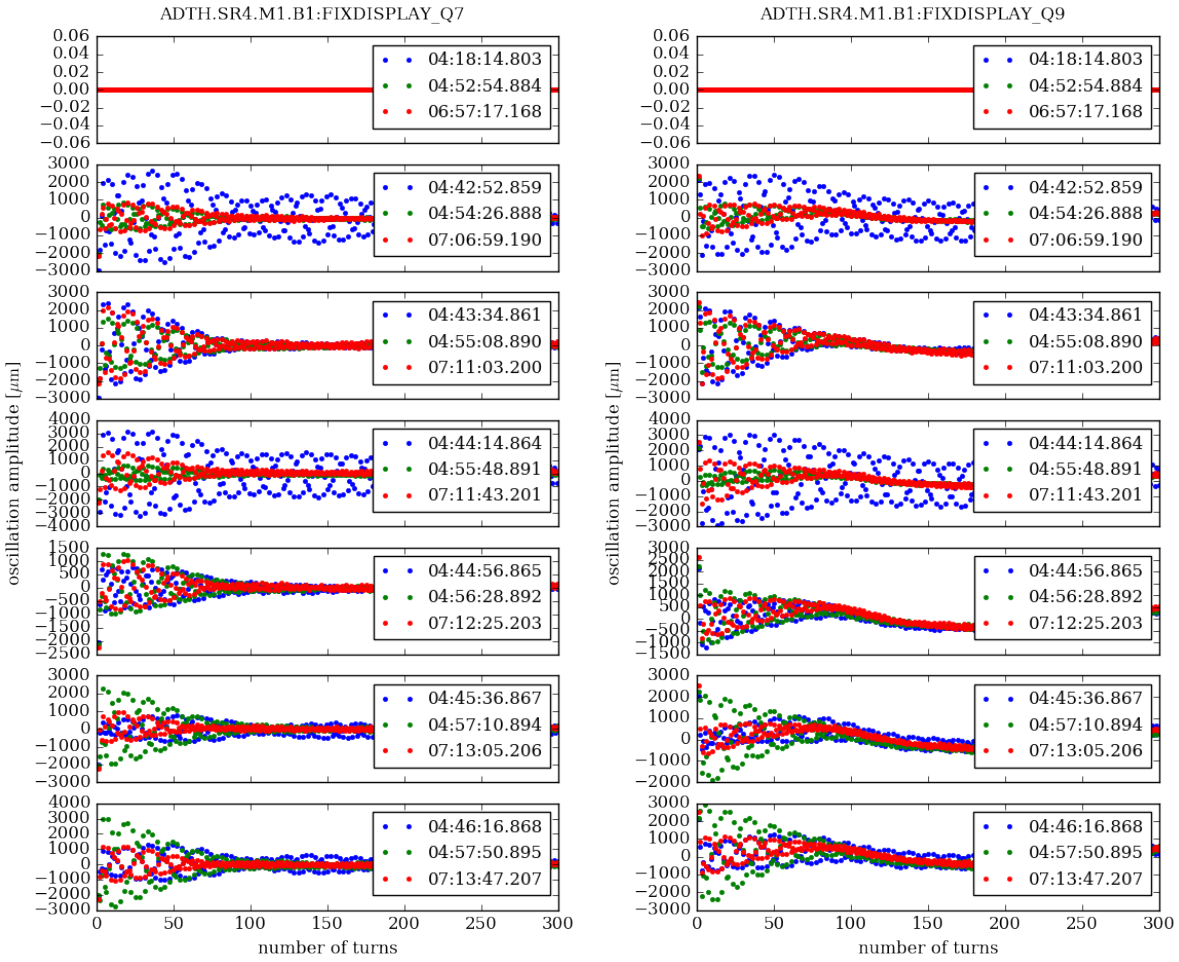

Figure 21: Injection oscillations in the horizontal plane for Beam 1 (weak beam) measured with the ADT pick-up at Q7 (left) and Q9 (right). Injection 1 is shown in green and Injection 2 is shown in red.

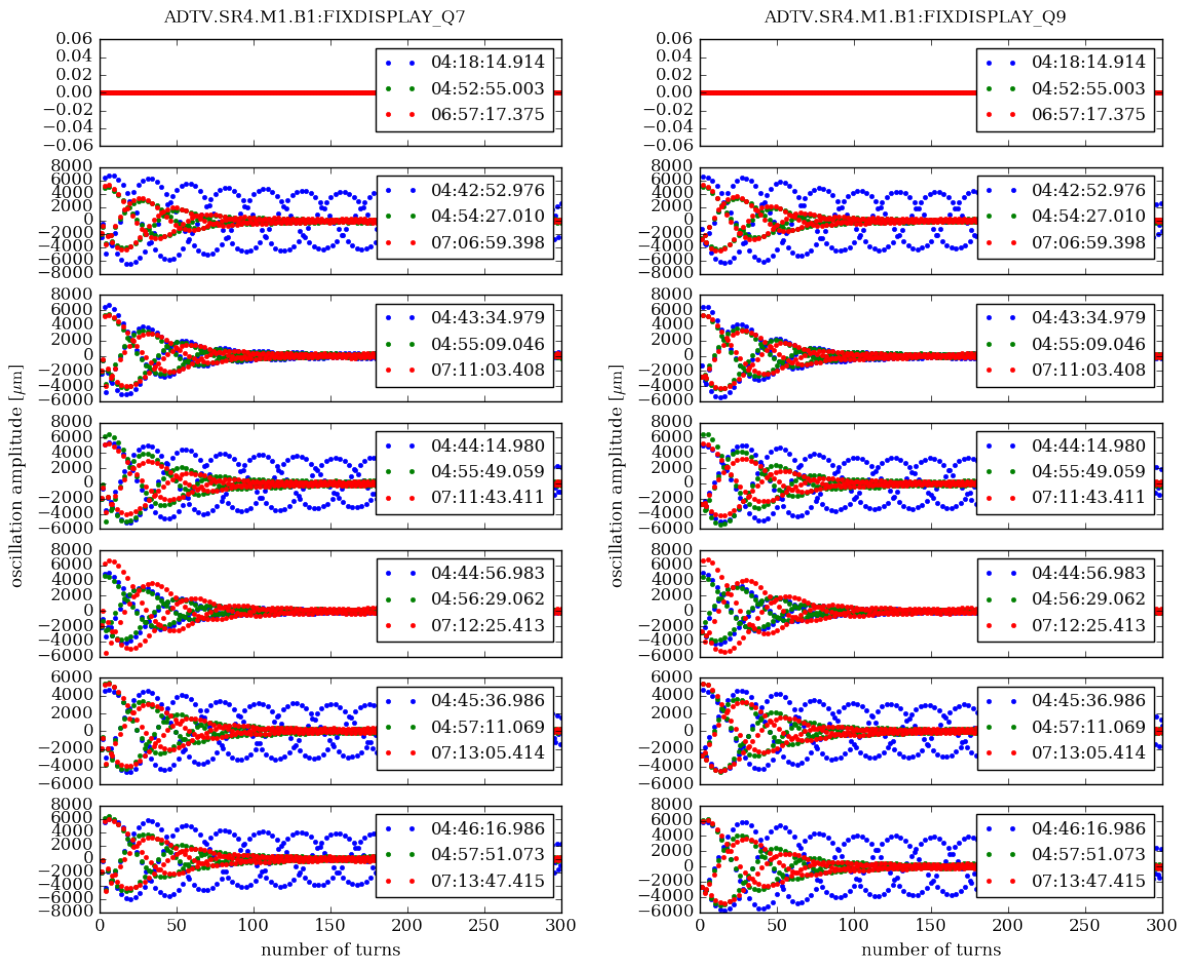

Figure 22: Injection oscillations in the vertical plane for Beam 1 (weak beam) measured with the ADT pick-up at Q7 (left) and Q9 (right). Injection 1 is shown in green and Injection 2 is shown in red.

BSRT profiles

A short introduction to the analysis of the BSRT profiles is given in Sec. 4 together with some typical plots at injection. In this section we want to concentrate on the impact of the low frequency excitation on the beam profiles and the possible differences between the two injections.

In presence of a low frequency excitation the profiles for different timestamps can not be averaged without subtracting the beam centroid. As no robust estimate for the centroid could be found, the direct profiles remain noisy and no effect of the low frequency excitation can be seen on the raw profiles nor residual or ratio.

The first statistical parameter to look at is the movement of the beam centroid under the influence of the low frequency excitation. The beam centroid can be defined by the center of gravity of the profile with

$$\text{cent}_{\text{gravity}} = \sum_{i=\text{bins}} x_i w_i \tag{18}$$

where x_i is the position of bin i and w_i the amplitude of bin i and is shown for both

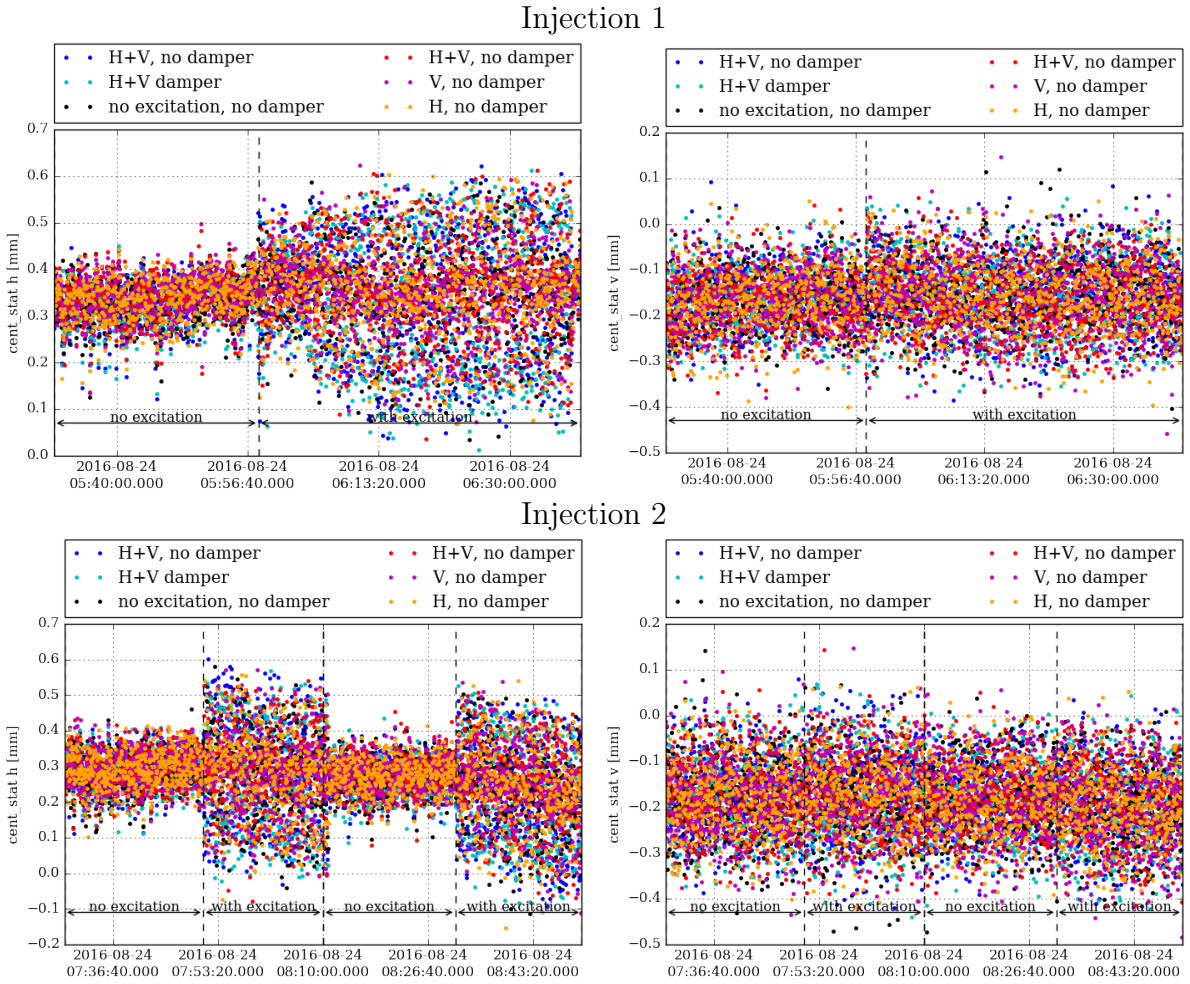

Figure 23: Horizontal (left) and vertical (right) position of the beam centroid $\text{cent}_{\text{gravity}}$ defined by Eqn. 18 for Injection 1 (top) and Injection 2 (bottom).

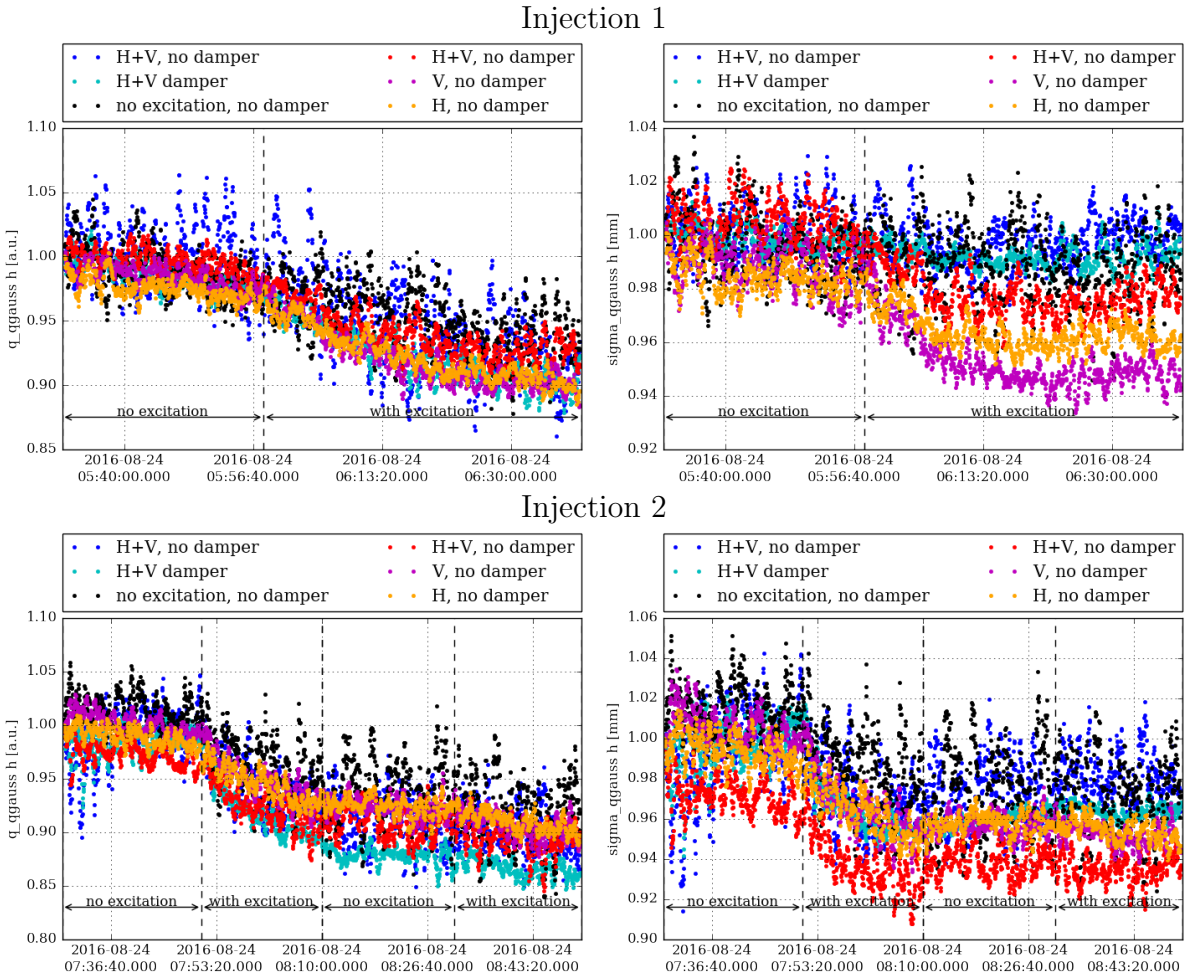

Figure 24: q-Gaussian fit parameters in the horizontal plane and Beam 1 (weak beam) for Injection 1 (top) and Injection 2 (bottom) normalized to the initial value and using a moving average over 10 consecutive time stamps.

injections in Fig. 23. The effect of the low frequency excitation on the closed orbit is visible in terms of a movement of the beam centroid in the horizontal plane. The vertical plane stays almost unchanged. The estimates of the centroid from the Gaussian and q-Gaussian fit show the same behavior. For Beam 2 the centroid stays unchanged. That the change of the beam centroid is only observed in the horizontal plane is unexpected as equal closed orbit distortions are expected in the horizontal and vertical plane (see Table 5) and with it comparable oscillations of the beam centroid.

As the beam distribution is often not Gaussian in the LHC, the Gaussian fit is often not a well suited model for the distribution. A new approach is to use instead a q-Gaussian fit as described in Sec. 4. For Beam 2 (strong beam) the σ and fit parameter c for the background in the vertical plane change sometimes but not reproducibly when the excitation is switched on (see Fig. 28–29). For Beam 1 (weak beam) all parameters stay unchanged when the low frequency excitation is switched on or off (see Fig. 27). Significant changes only occur in the horizontal plane of Beam 1 (see Fig. 24). In contradiction to the observed emittance growth in the BSRT emittance extracted from the

Table 5: Closed orbit distortion at the location of the BSRT due to an excitation with the maximum ADT kick amplitude of 0.481 μrad per module with in total four modules per beam. Parameters are injection optics ($\beta^* = 11.0$ m) with collision tunes.

ADT pickup	x_{BSRT} [mm]	y_{BSRT} [mm]
BSRTR.5R4.B1	0.22	0.22
BSRTM.5R4.B1	0.23	0.23

Logging database (see Fig. 14–15), a decrease of the beam sigma is seen when the low frequency excitation is switched on the first time. This results is consistent with the hypothesis that a low frequency excitation actually does *not* result in emittance growth. The beam size and also the q-parameter decreases as the tails are scraped due to the closed orbit distortion induced by the low frequency excitation. In case of the BSRT emittance obtained from the Logging database, the emittance growth is probably due to the Gaussian fit and a wrong or no subtraction of the beam centroid. This hypothesis is substantiated by the fact, that the movement of the beam centroid is only visible in the horizontal plane (see Fig. 23), which is also the plane for which the emittance growth is observed. Assuming a Gaussian fit as defined in Eqn. 7, the statistical parameters as summarized in Appendix C are obtained.

Further analysis

Except for the data acquired with the diamond BLMs and the scraping with the collimators when the beam was dumped all relevant data has been analyzed. A further and more detailed analysis of the loss pattern could reveal why losses due to a low frequency excitation are observed during Injection 2, but not during Injection 1.

Summary

During this MD a low frequency excitation was tried in two consecutive fills, for which an identical setup was chosen. However, the two injections yielded different results:

Injection 1: A low frequency excitation in the horizontal plane (or horizontal and vertical) leads to emittance growth for colliding and non-colliding bunches. This emittance growth can be mitigated with the transverse damper. No increase of beam losses is observed.

Injection 2: A low frequency excitation in the horizontal plane (or horizontal and vertical) leads to beam losses for colliding and non-colliding bunches. These losses can *not* be mitigated with the transverse damper. The emittance change observed, is most likely a convolution of the beam distribution change due to the excitation (resulting in an increase of the emittance) and due to the losses (resulting in a decrease of emittance). Therefore no conclusion concerning the emittance growth can be drawn.

In Sec. 5.4 an attempt is made to find out the reason for the different results for the two injections, however with limited success. The following possible reasons were investigated:

- **Change of tune and chromaticity:** Any change is highly unlikely (see Sec. 3.1)
- **Orbit drifts at TCPs:** The BPMs close to the TCPs do not show any significant changes (see Sec. 5.4.1).
- **Change of emittance:** In case of a larger emittance and thus larger beam size, any orbit distortions would cut deeper into the beam distribution (see Fig. 25 for a sketch of the effect) and thus would result in higher losses. However, the emittances in Injection 2 were smaller than in Injection 1, which is the opposite to be expected based on this reasoning (see Sec. 5.1, Fig. 12).

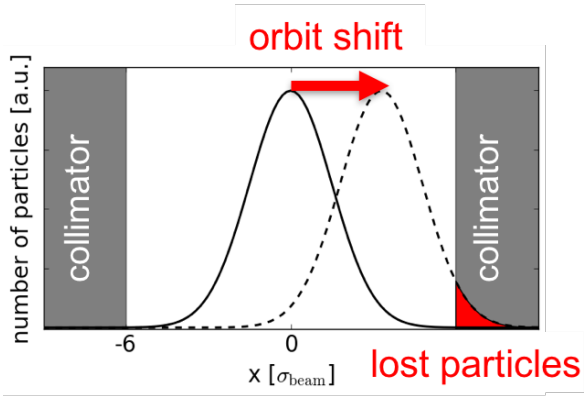

Figure 25: Sketch of loss mechanism in case of orbit distortions.

- **Measurement error in FBCTs:** The BLMs at the TCPs show the same result as the FBCT measurements (see Sec. 5.4.2). Explicitly, no increase of losses with low frequency excitation for Injection 1 and an increase of losses with low frequency excitation for Injection 2.
- **Injection oscillations:** Larger injection oscillations could lead to a difference in the tail population. The injection oscillations as measured with the ADT are very similar for the two injections and this reason can thus also be ruled out (see Sec. 5.4.3)
- **BSRT emittance and transverse distribution change:** In addition to the emittance values saved in the LHC Logging database, also the transverse beam profiles from the BSRT were saved and analyzed (see Sec. 5.4.4). Using the model of a q-Gaussian fit, the analysis reveals a decrease of the beam sigma due to the low frequency excitation. Based on the direct analysis of the profiles and the observation that the centroid moves mostly in the horizontal plane, the emittance growth seen in Fig. 14–15 is most likely artificial due to the Gaussian fit of the profile taking not correctly the centroid into account.

Outlook

The MD should be repeated as it yields very confusing results. A more detailed check of the BBQ spectra could be made to recheck tune and chromaticity.

References

[1] M. Fitterer, M. Albert, F. Antoniou, et al. *Effect of low frequency noise on the evolution of the emittance and halo population*. Tech. rep. CERN-ACC-NOTE-2016-0029. CERN, 2016. URL: http://cds.cern.ch/record/2135147.

[2] V. A. Lebedev. "Emittance growth due to noise and its suppression with the feedback system in large hadron colliders". In: *Proceedings, Accelerator Physics at the Superconducting Super Collider, AIP Conf. Proc.* 326.SSCL-PREPRINT-188 (1995), pp. 396–423. DOI: 10.1063/1.47298. URL: http://inspirehep.net/record/353807?ln=en.

[3] Y. Alexahin. "On the emittance growth due to noise in hadron colliders and methods of its suppression". In: *Nuclear Instruments and Methods in Physics Research Section A: Accelerators, Spectrometers, Detectors and Associated Equipment* 391.1 (1997), pp. 73 –76. ISSN: 0168-9002. URL: http://www.sciencedirect.com/science/article/pii/S0168900296011904.

[4] K. Ohmi, R. Calaga, R. Tomas, et al. "Beam-beam effect with an external noise in LHC". In: *Conf. Proc. PAC'07* C070625.PAC07-TUPAN048 (2007), p. 1496.

[5] K. Ohmi. "Beam-beam effects under the influence of external noise". In: *Proceedings, ICFA Mini-Workshop on Beam-Beam Effects in Hadron Colliders (BB2013): CERN, Geneva, Switzerland, March 18-22 2013*. [,69(2014)]. 2014, pp. 69–74. arXiv: 1410.4092 [physics.acc-ph]. URL: http://inspirehep.net/record/1322414/files/arXiv:1410.4092.pdf.

[6] J. Qiang. *Updates on Simulation of Noise Effects Using BeamBeam3D*. Beam-Beam and Luminosity Studies meeting. 2015. URL: https://indico.cern.ch/event/448921/.

[7] J. Qiang. *Impact of Noise on Beam Quality*. Joint LARP CM28/HiLumi Meeting. Apr. 25, 2017. URL: https://conferences.lbl.gov/event/76/timetable/#20170425.

[8] *private communication F. Antoniou*.

[9] R. Brinkmann and F. Willeke. "First experience with colliding electron-proton beams in HERA". In: *Proceedings of International Conference on Particle Accelerators*. 1993, 3742–3744 vol.5.

[10] *private communication E. Métral*.

[11] M. Guinchard. *Vibration analysis of TT41 TAG41*. 16th HL-LHC Parameter and Layout Commitee Metting. URL: https://indico.cern.ch/event/406292/.

[12] M. Fitterer, G. Stancari, A. Valishev, et al. *Effect of a resonant excitation on the evolution of the beam emittance and halo population*. Tech. rep. CERN-ACC-NOTE-2017-0037. 2017. URL: https://cds.cern.ch/record/2264616.

[13] D. Valuch. *ADT operation. A cook book of black magic*. LBOC Meeting No 61. URL: https://indico.cern.ch/event/527889/.

[14] M. Fitterer, F. Antoniou, G. Stancari, et al. *Analysis of BSRT profiles in the LHC at injection*. Tech. rep. to be published. Fermilab, Feb. 2017.

[15] G. Trad. “Development and Optimisation of the SPS and LHC beam diagnostics based on Synchrotron Radiation monitors”. PhD Thesis, CERN. University of Grenoble. URL: https://tel.archives-ouvertes.fr/tel-01157800/document.

q-parameter without excitation during Injection 2

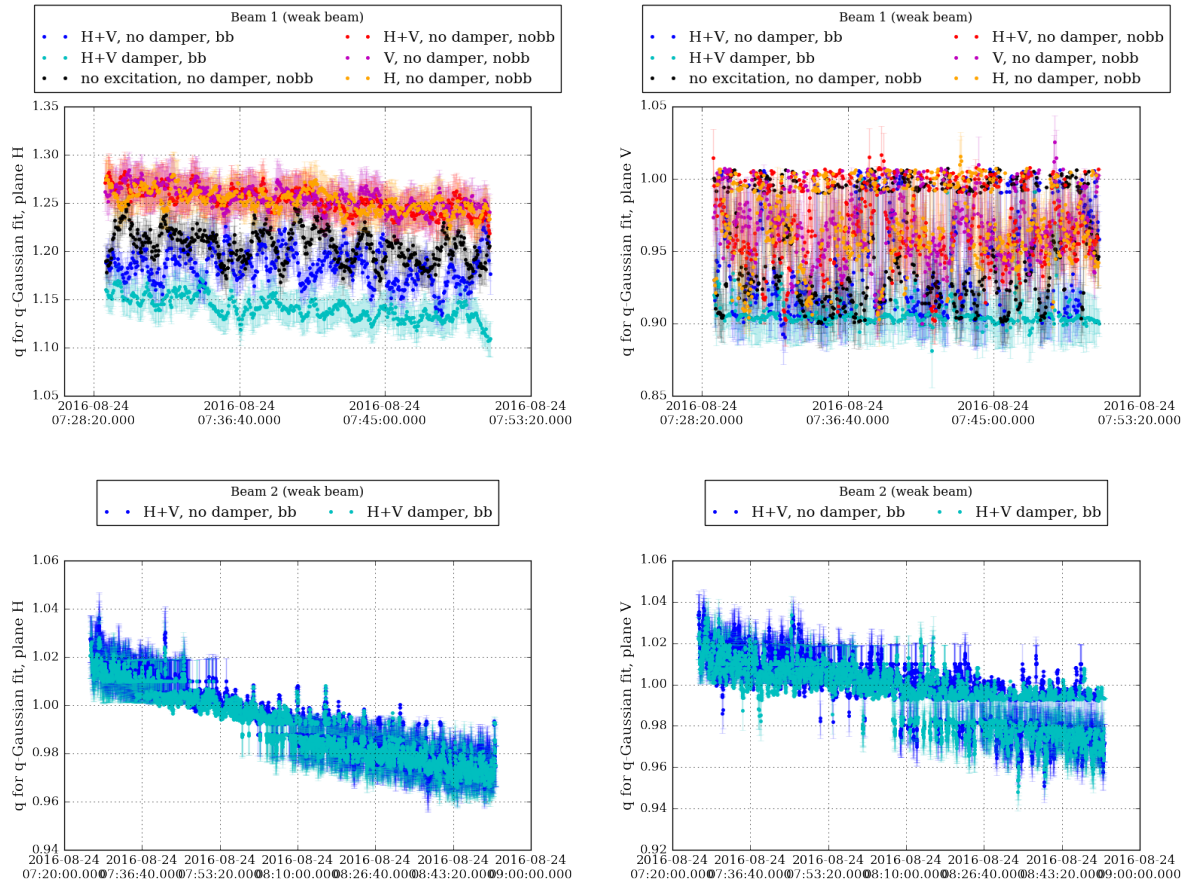

Figure 26: q parameter of q-Gaussian fit in the horizontal (left) and vertical (right) plane: q-parameter without excitation during Injection 2 in fill 5244 for Beam 1 and during the entire Injection 2 for Beam 2. Beam 1 (weak beam) is shown on the top and and Beam 2 (strong beam) is shown on the bottom. The bunches of Beam 2 are both colliding and are labeled according to their partners in Beam 1. For Beam 2 no excitation is applied and the transverse damper is active for both bunches. The q-Gaussian fit is performed for the average profiles and without background subtraction. The errorbars contain only the error from the q-Gaussian fit obtained from the covariance matrix ($\sigma_q = \sqrt{(\mathrm{cov}(p_q, p_q)}$ where p_q indicates the diagonal element of the matrix for the fit parameter q).

q-Gaussian fit parameters for Injection 1 and Injection 2

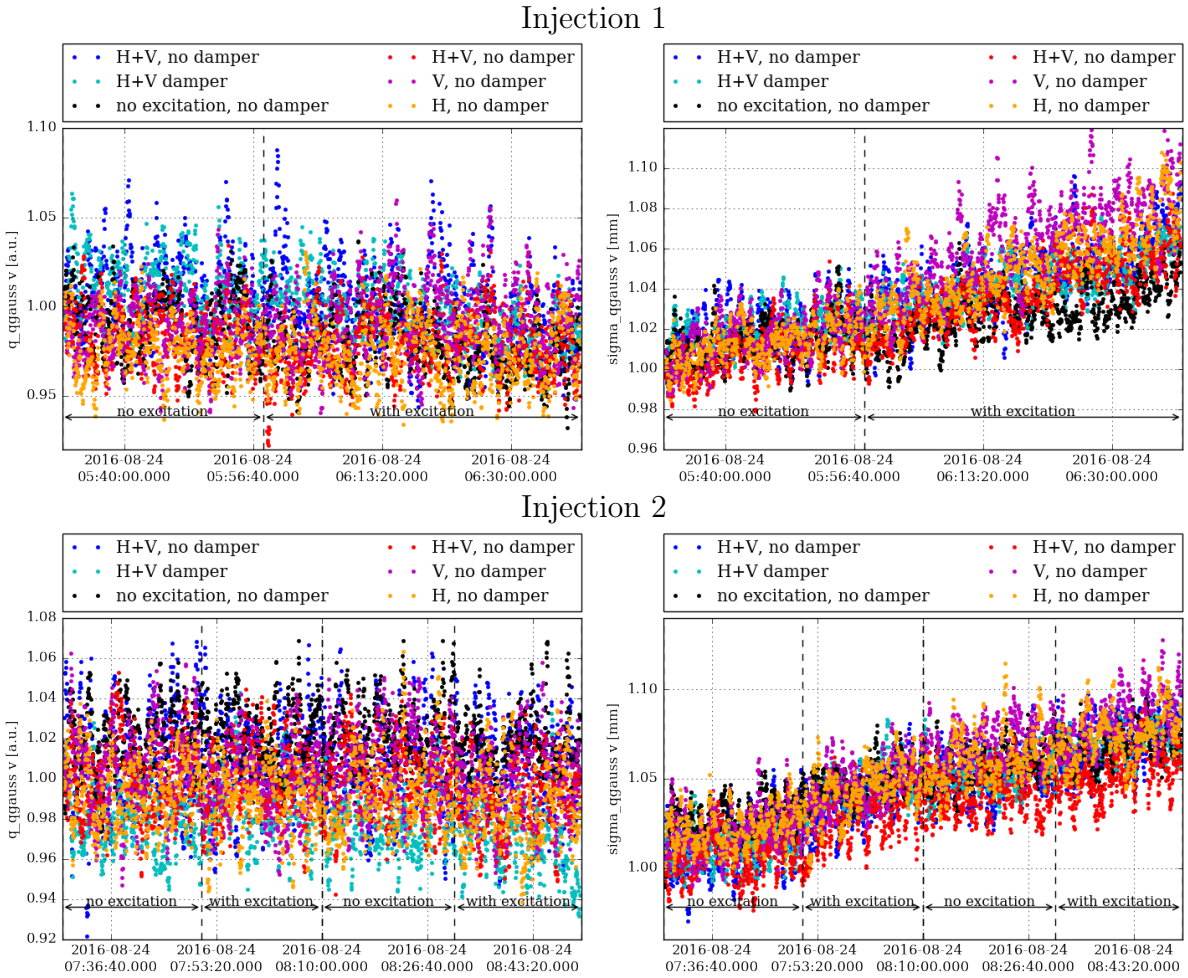

Figure 27: q-Gaussian fit parameters in the vertical plane and Beam 1 (weak beam) for Injection 1 (top) and Injection 2 (bottom) normalized to the initial value and using a moving average over 10 consecutive time stamps.

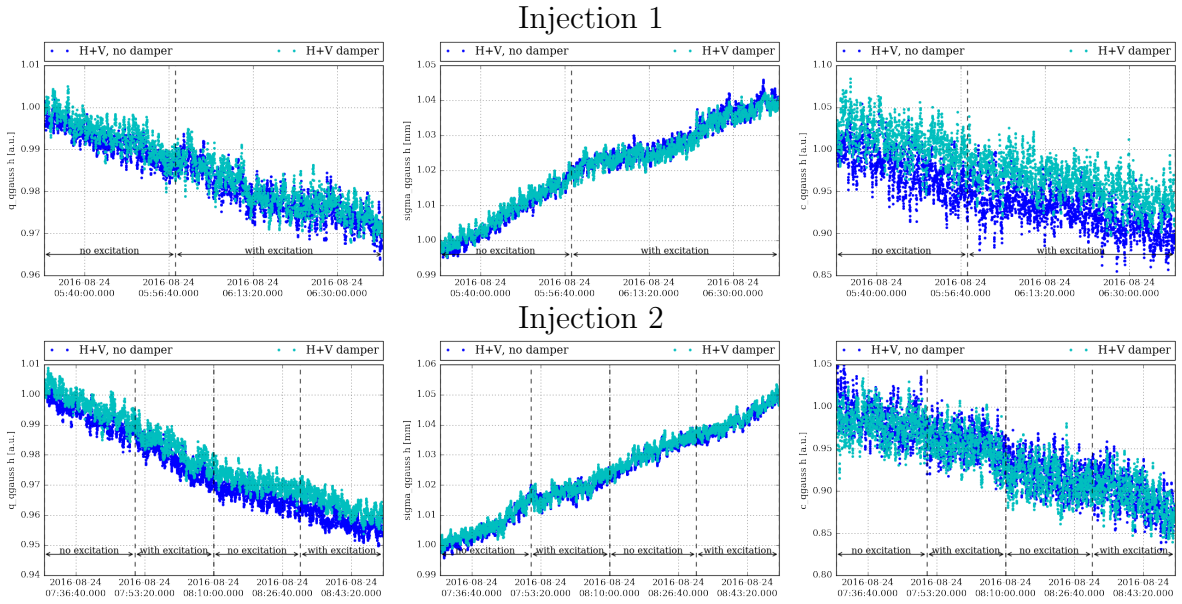

Figure 28: q-Gaussian fit parameters in the horizontal plane and Beam 2 (strong beam) for Injection 1 (top) and Injection 2 (bottom) normalized to the initial value and using a moving average over 10 consecutive time stamps.

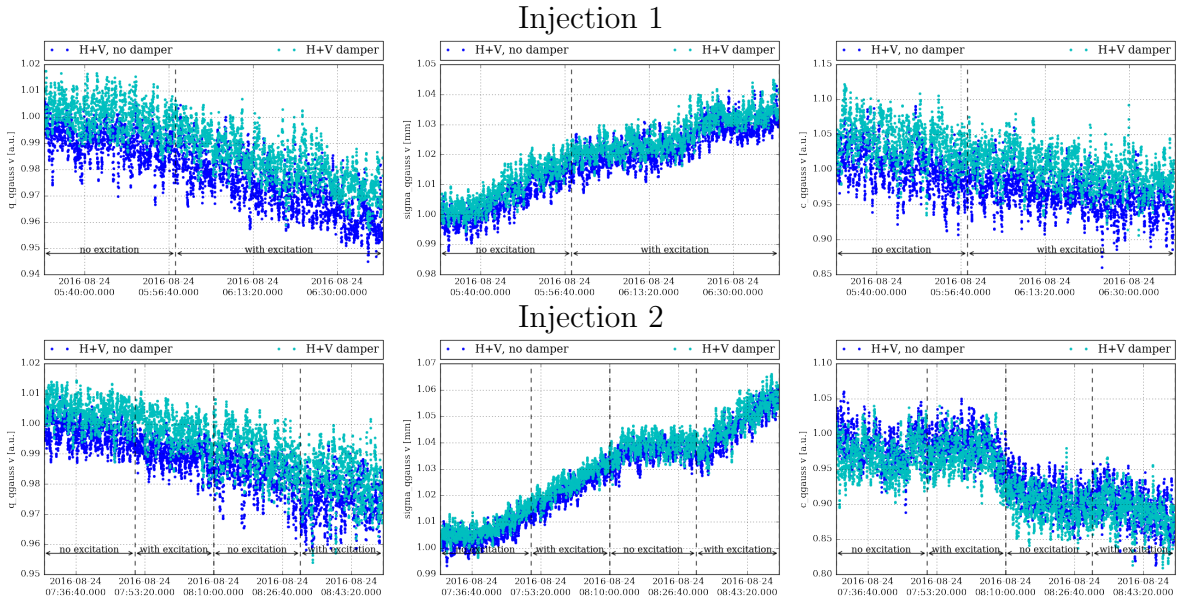

Figure 29: q-Gaussian fit parameters in the vertical plane and Beam 2 (strong beam) for Injection 1 (top) and Injection 2 (bottom) normalized to the initial value and using a moving average over 10 consecutive time stamps.

Gaussian fit parameters for Injection 1 and Injection 2

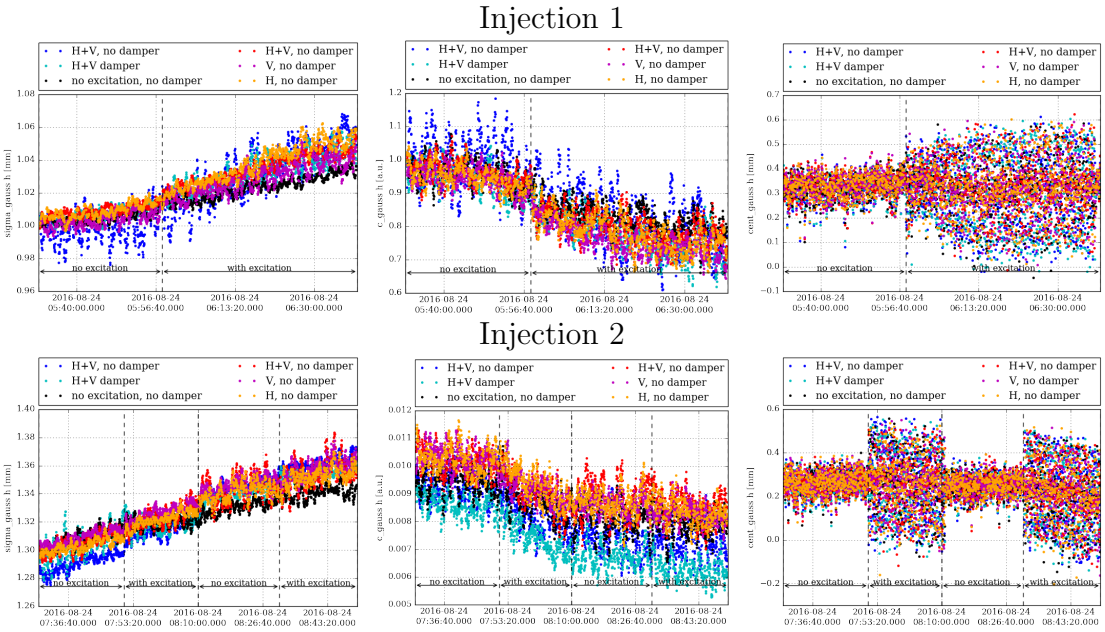

Figure 30: Gaussian fit parameters in the horizontal plane and Beam 1 (weak beam) for Injection 1 (top) and Injection 2 (bottom). The centroid cent_gauss is not averaged. The σ sigma_gauss and the fit parameter for the background c_gauss are calculated using a moving average over 10 consecutive time stamps and normalized to the initial value.

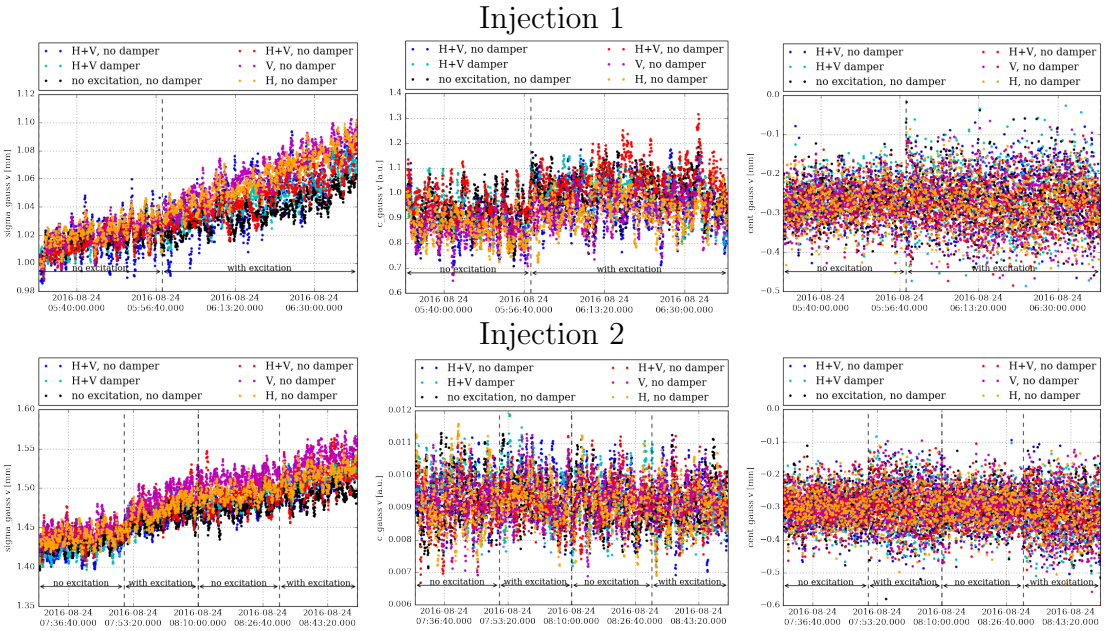

Figure 31: Gaussian fit parameters in the vertical plane and Beam 1 (weak beam) for Injection 1 (top) and Injection 2 (bottom). The centroid cent_gauss is not averaged. The σ sigma_gauss and the fit parameter for the background c_gauss are calculated using a moving average over 10 consecutive time stamps and normalized to the initial value.

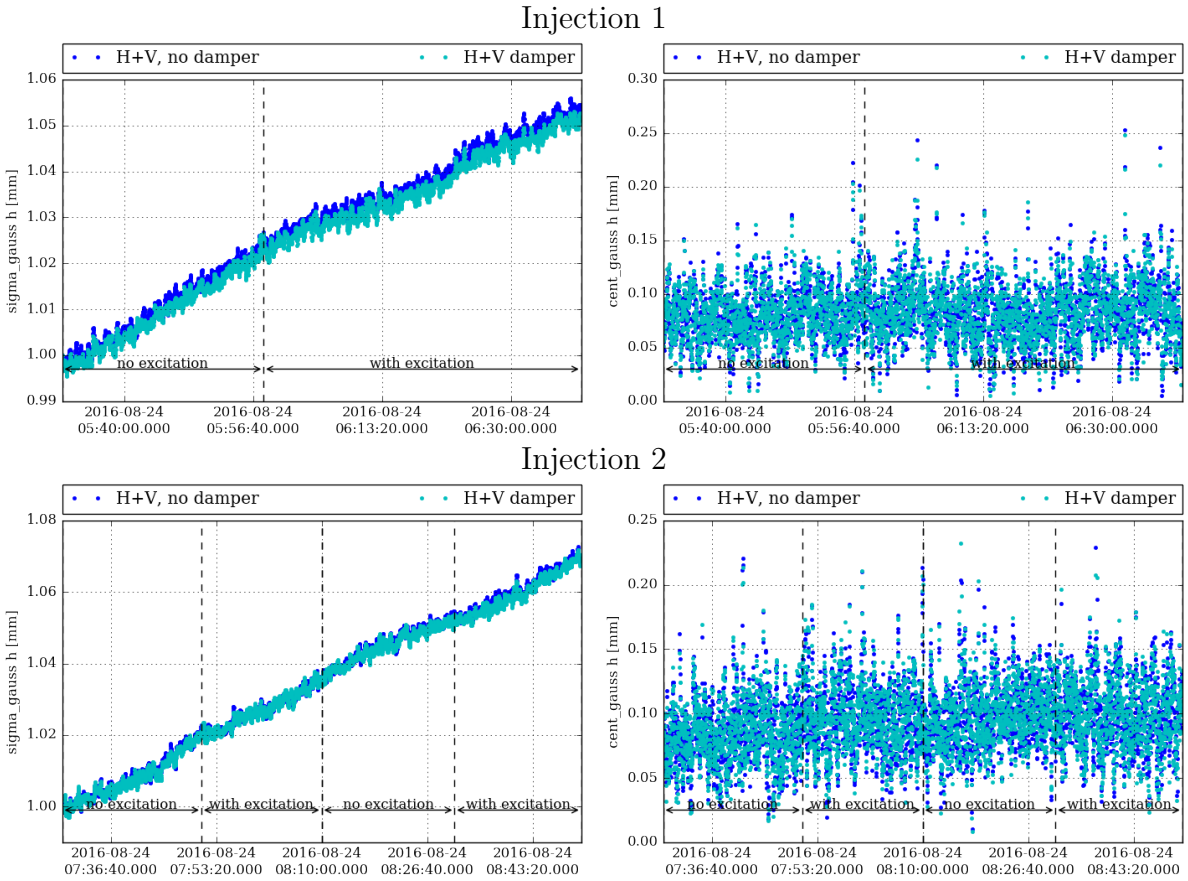

Figure 32: Gaussian fit parameters in the horizontal plane and Beam 2 (strong beam) for Injection 1 (top) and Injection 2 (bottom). The centroid cent_gauss is not averaged. The σ sigma_gauss is calculated using a moving average over 10 consecutive time stamps and normalized to the initial value.

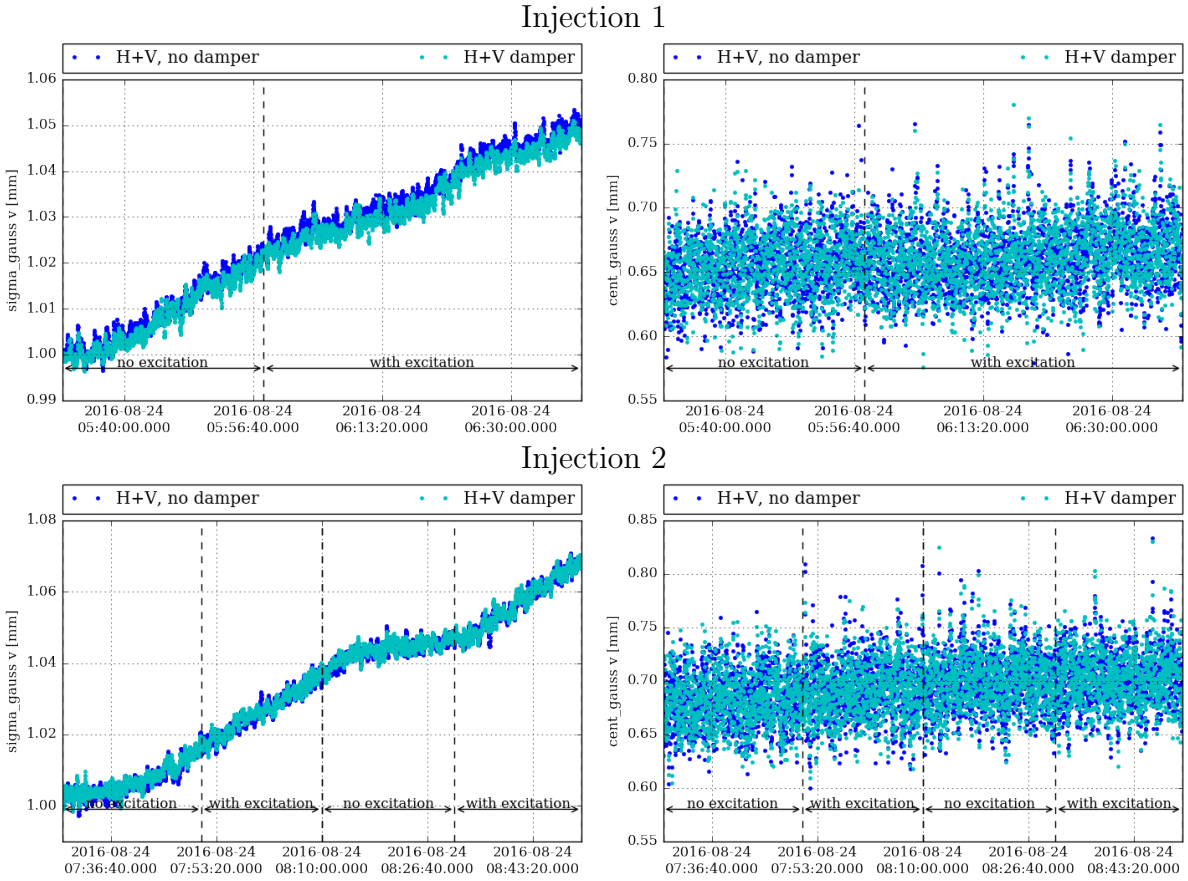

Figure 33: Gaussian fit parameters in the vertical plane and Beam 2 (strong beam) for Injection 1 (top) and Injection 2 (bottom). The centroid cent_gauss is not averaged. The σ sigma_gauss is calculated using a moving average over 10 consecutive time stamps and normalized to the initial value.